Bioorganic Chemistry 148 (2024) 107462

Contents lists available at ScienceDirect

Bioorganic Chemistry

journal homepage: www.elsevier.com/locate/bioorg

Exploring flavylium-based SWIR emitters: Design, synthesis and optical characterization of dyes derivatized with polar moieties

Federica Blua [a,*], Mariangela Boccalon [b], Barbara Rolando [a], Roberta Napolitano [b], Francesca Arena [b], Francesco Blasi [b], Massimo Bertinaria [a]

[a] Department of Drug Science and Technology, University of Turin, Turin, Italy
[b] Bracco Research Center, Bracco Imaging S.p.A, Colleretto Giacosa (Turin), Italy

ARTICLE INFO

Keywords:
Shortwave infrared
Polymethine dyes
Flavylium fluorophores
Optical imaging
SWIR emitters

ABSTRACT

Imaging in the shortwave infrared (SWIR, 1000–1700 nm) region is gaining traction for biomedical applications, leading to an in-depth search for fluorophores emitting at these wavelengths. The development of SWIR emitters, to be used *in vivo* in biological media, is mostly hampered by the considerable lipophilicity of the structures, resulting from the highly conjugated scaffold required to shift the emission to this region, that limit their aqueous solubility. In this work, we have modulated a known SWIR emitter, named **Flav7**, by adding hydrophilic moieties to the flavylium scaffold and we developed a new series of **Flav7**-derivatives, which proved to be indeed more polar than the parent compound, but still not freely water-soluble. Optical characterization of these derivatives allowed us to select **FlavMorpho**, a new compound with improved emission properties compared to **Flav7**. Encapsulation of the two compounds in micelles resulted in water-soluble SWIR emitters, with **FlavMorpho** micelles being twice as emissive as **Flav7** micelles. The SWIR emission extent of **FlavMorpho** micelles proved also superior to the tail-emission of Indocyanine Green (ICG), the FDA-approved reference cyanine, in the same region, by exciting the probes at their respective absorption maxima in phosphate buffered saline (PBS) solution. The availability of optical imaging devices equipped with lasers able to excite these dyes at their maximum of absorption in the SWIR region, could pave the way for implemented SWIR imaging results.

1. Introduction

In recent years, fluorescence-based optical imaging has emerged as a powerful intraoperative diagnostic tool [1–3], with fluorescence-guided surgery (FGS) being the most interesting clinical application of this technique. Indeed, being able to visualize the localization of tumours, thanks to the specific accumulation of fluorescent probes within them, could improve solid tumour removal [4–6]. The advantages of using fluorophores able to emit light in the shortwave infrared (SWIR, also called near-infrared region II or NIR-II, 1000–1700 nm) region of the electromagnetic spectrum over the visible (VIS, 400–700 nm) or the near-infrared region I (NIR-I, 700–1000 nm, Fig. 1A) have been recently highlighted. Major advantages of SWIR imaging can be attributed to reduced background autofluorescence, reduced tissue scattering, and increased penetration depth of the photons at these wavelengths, resulting in improved image quality and higher resolution [7,8]. Starting from the first developed SWIR emitters, mainly represented by inorganic single-walled carbon nanotubes [9], many other inorganic and organic materials have been developed, with the latter being preferred for a better safety profile [10–12].

The search for small-molecular organic fluorophores capable of emitting in the SWIR region has attracted increasing interest in the last decade [13,14]. Currently, the most promising SWIR emitters can be found among the exponents of mainly three categories of fluorophores, which are donor–acceptor–donor (D-A-D) compounds, polymethine dyes and boron-dipyrromethene (BODIPY) dyes [10,15–17]. Polymethine fluorophores have been extensively studied and investigated due to their favourable photophysical properties, such as high molar extinction coefficients (ε) and moderate fluorescence quantum yield (Φ_F) [18–20]. Among them, cyanine dyes, consisting of two *N*-containing heterocycles linked by a polymethine bridge of variable length, were originally developed as NIR-I emitters, with indocyanine green (ICG) being the best-known representative and the first FDA-approved fluorophore (Fig. 1B). Over the years, cyanine dyes have undergone wide

* Corresponding author.
E-mail address: federica.blua@unito.it (F. Blua).

https://doi.org/10.1016/j.bioorg.2024.107462
Received 18 March 2024; Received in revised form 3 May 2024; Accepted 14 May 2024
Available online 17 May 2024

chemical modulation to shift their emission towards the NIR-II region [14,18].

Among the strategies adopted to shift the emission wavelength, the replacement of the *N*-containing heterocycles on the polymethine bridge, with the aim to enhance their donor-strength behaviour, has led to the development of new SWIR emitters, such as Flav [21], BTC [22] and CX-derivatives [23], also collectively referred to as cyanine-like compounds (Fig. 1B).

One of the first cyanine-like compounds to exhibit interesting optical properties was Flav7, a flavylium polymethine derivative developed by Sletten and co-workers [21]. The introduction of the electron-donating dimethylamino group on the flavylium scaffold promoted the shift of the absorption and emission wavelengths to the SWIR region; moreover, this new derivative showed a high brightness and the highest fluorescence quantum yield (Φ_F) value compared with the aforementioned NIR-II emitters modified on the heterocycles (Fig. 1B). Over the years, the same group has proposed various modifications of the flavylium scaffold, developing new compounds with similar or better optical properties compared to the parent compound Flav7 [24,25]. However, all these newly developed dyes share the same limitation, consisting of extremely poor solubility in water due to the high lipophilicity and significant flatness of their structures, which restrain their application in polar environments. The structural planarity and low water solubility promote intermolecular π-π stacking interactions, which usually favour self-aggregation phenomena in water. Depending on the mutual arrangement of the molecules acquired during the aggregation process, different types of aggregate forms are possible [26–28]. Often, these molecules acquire a parallel, face-to-face arrangement, generating the so-called H-aggregates, which are characterized by a higher energy transition resulting in a broad, blue-shifted absorption band. The formation of this type of aggregates is usually responsible for the aggregation-caused quenching (ACQ) effect, which consists of diminished or quenched fluorescence emission, due to the non-radiative dissipation of the energy absorbed by the aggregated species. As a result of these phenomena, a decline in fluorescence quantum yield (Φ_F) is commonly observed for these organic π-conjugated materials in aqueous media, which therefore undermines their application in biological environments [28].

An approach to increase water solubility consists in the addition of polar or hydrophilic groups on the dye scaffold. Another strategy, which has shown good promises for clinical biological application, consists in the encapsulation of lipophilic dyes in nanosystems, such as micelles or other carriers [18].

In this work, in order to obtain new derivatives endowed with improved optical properties in polar environments, we explored both the aforementioned strategies. First, we modified the structure of Flav7 by introducing polar *N*-containing heterocycles at the 7-position of the flavylium ring, developing a versatile new synthetic procedure. Then, one compound, FlavMorpho (**1**), selected among the others for its better optical properties, was encapsulated in phospholipidic micelles, and

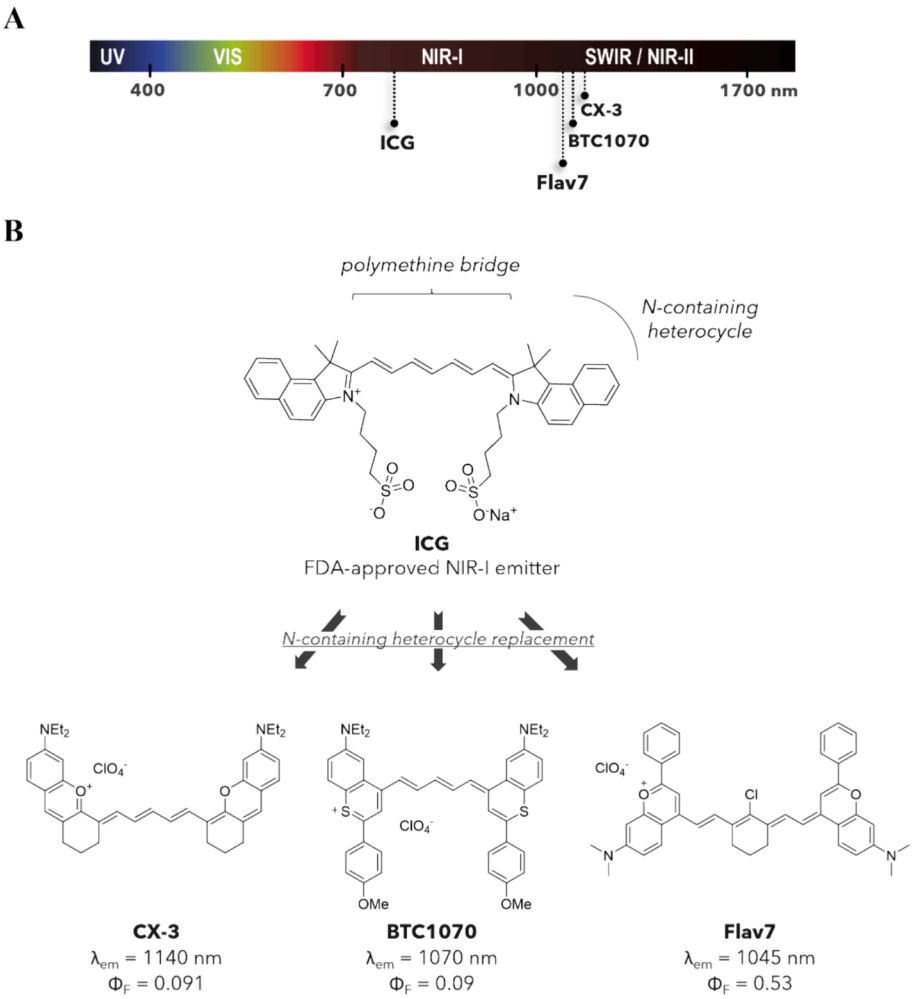

Fig. 1. (A) Regions of the electromagnetic spectrum with fluorophores reported in correspondence with their emission wavelengths. (B) Structure of reference indocyanine green (ICG) and new SWIR emitters obtained after replacement of *N*-containing heterocycles. Emission wavelengths (λ_{em}) and fluorescence quantum yields (Φ_F) reported from literature [21–23].

employed for preliminary optical imaging experiments. The design, synthesis and optical characterization of these new compounds are here discussed.

2. Results and discussion

2.1. Design and synthesis of new fluorophores

Based on the observation that position 7 of the flavylium ring of Flav7 was the most suitable for derivatization [29], we decided to replace the dimethylamino moiety of the parent compound with other different amino groups. In order to investigate how different properties in terms of polarity and ionization may influence the optical behaviour of the fluorophores, we selected a series of cyclic and linear amino groups to derivatize the flavylium scaffold, and we designed the compounds reported in Fig. 2. For all the designed derivatives, the electron-donating capability of the amino group was maintained. To increase the polarity, we firstly replaced the dimethylamino group with a morpholine residue, capable of establishing more hydrogen bonds in polar environments, and we designed compound **1**. Substituents with ionizable groups in water or biological media were then investigated. Compounds **2** and **3** were thus obtained by adding a piperazine or a *N*-methylpiperazine moiety, respectively, providing positive charges on the scaffold. To obtain negatively charged compounds in aqueous environments, an isonipecotic acid and a 2-methylaminoethanesulfonic acid substructures were used instead, developing compounds **4** and **6**, respectively. Compound **5**, bearing a 4-(piperazin-1-yl)butanesulfonic acid as substituent and most likely present in aqueous solution in zwitterionic form, was also designed.

Compounds **1**–**5**, with cyclic amino groups as substituents, were obtained by developing a new synthetic procedure reported in Scheme 1. Using the same synthetic approach, we were also able to obtain substituted compounds with linear amino groups (such as **Flav7**, our reference compound, and **6**, Scheme 2), demonstrating that this is a versatile new procedure that can derivatize the scaffold with several and structurally different amines. In both cases (Schemes 1 and 2), the same fluorine-containing precursor **7** was reacted with cyclic (**8**–**11**) or linear (**24**–**25**) amines to give, through nucleophilic substitution, the respective amino-substituted compounds **12**–**15** and **26**–**27** in good yields. These intermediates were cyclized with acetophenone **17** under acidic conditions to obtain the substituted flavylium cations **18**–**21** and **28**–**29**, which were then reacted with the bis(phenylimino) derivative **23** to give the final compounds **1**–**4**, **6** and **Flav7**. To obtain the final compound **5**, intermediate **15** was instead submitted to alkylation with 1,4-butanesultone, obtaining compound **16** in satisfactory yields. This derivative then underwent the same synthetic steps consisting in acid-mediated cyclization to give compound **22** followed by reaction with **23** to obtain the desired compound **5**.

Since **Flav7** derivatives reported to date have been prepared by using always distinct procedures, the ability to obtain all the designed products from the same precursor and by using the same synthetic steps has represented a major advantage. Furthermore, this new procedure avoids the critical steps related to the use of harsh and potentially explosive reaction conditions as in previously reported synthetic routes [21,24].

However, while dealing with these compounds, we encountered some difficulties when performing the last reaction step, as many by-products were formed simultaneously, and it was quite challenging to isolate the pure final compounds. While products **1**–**4** and **Flav7** were obtained with a purity higher than 96 %, compounds **5** and **6** were still contaminated by the presence of the hemicyanine by-product (detected at $\lambda = 500$ nm and identified by HPLC-MS analysis, see Fig. S1 for compound **6**), which could not be eliminated even by using semi-preparative high-performance liquid chromatography (HPLC). Final purity of these two compounds at 254 nm was 71 % and 82 % respectively, and since the presence of the hemicyanine by-product can influence the absorption and emission behaviour, they were not characterized further for their optical properties.

2.2. Photophysical properties of new derivatives

Compounds **1**–**4** and **Flav7** were characterized for their optical properties. Absorption and emission spectra were recorded in solvents with different polarities. All the newly synthesized compounds, analyzed at the same concentration (20 μM), behaved as SWIR emitters in organic solvents, with an emission wavelength beyond 1000 nm. No substantial hypso- or bathochromic shifts in emission wavelengths compared to parent compound **Flav7** were evidenced in organic solvents (Table S1). Absorption and emission spectra in dichloromethane (DCM) and acetonitrile (ACN) are reported in Fig. 3. Solvatochromic effect (i.e. the dependence of the optical properties upon the solvent) in the absorption spectrum was evidenced for compound **2** in DCM (Fig. 3A) and for all the compounds in a more polar solvent such as ACN, since a broad absorption shoulder was recorded at shorter wavelengths (Fig. 3C). In both solvents, compound **1** (**FlavMorpho**) was the most emissive derivative, even more emissive than the parent compound **Flav7** (Fig. 3B, D).

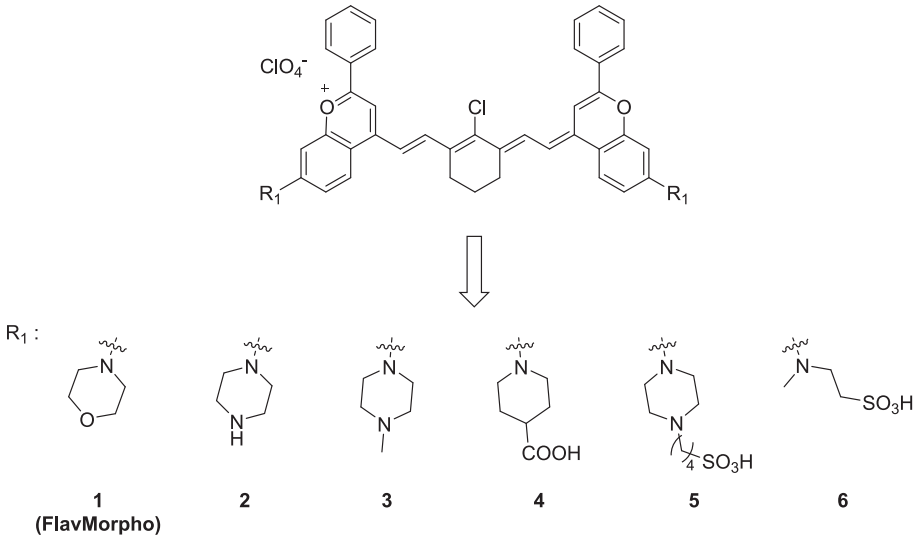

Fig. 2. Structures of designed and synthesized Flav7-derivatives.

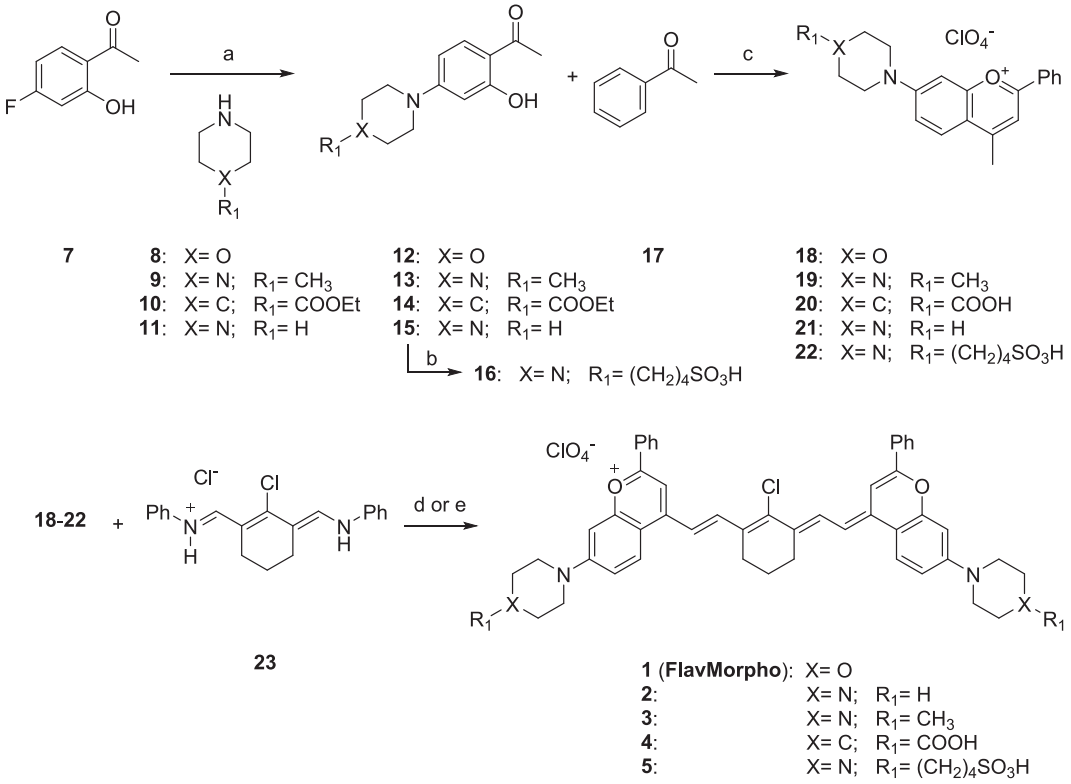

Scheme 1. Reagents and conditions: (a) 110–130 °C, 2–3 h, 65–90 %. (b) 1,4-butanesultone, 1,4-dioxane, 95 °C, 24 h, 89 %. (c) $HClO_4$ 70 %, CH_3COOH, 105 °C, 20 h, 30–70 %. (d) 2,4,6-trimethylpyridine or NaOAc, *n*-BuOH/Toluene, 100 °C, 1–5 h, 21–35 %. (e) NaOAc, Acetic anhydride, 80 °C, 2 h, 22 %.

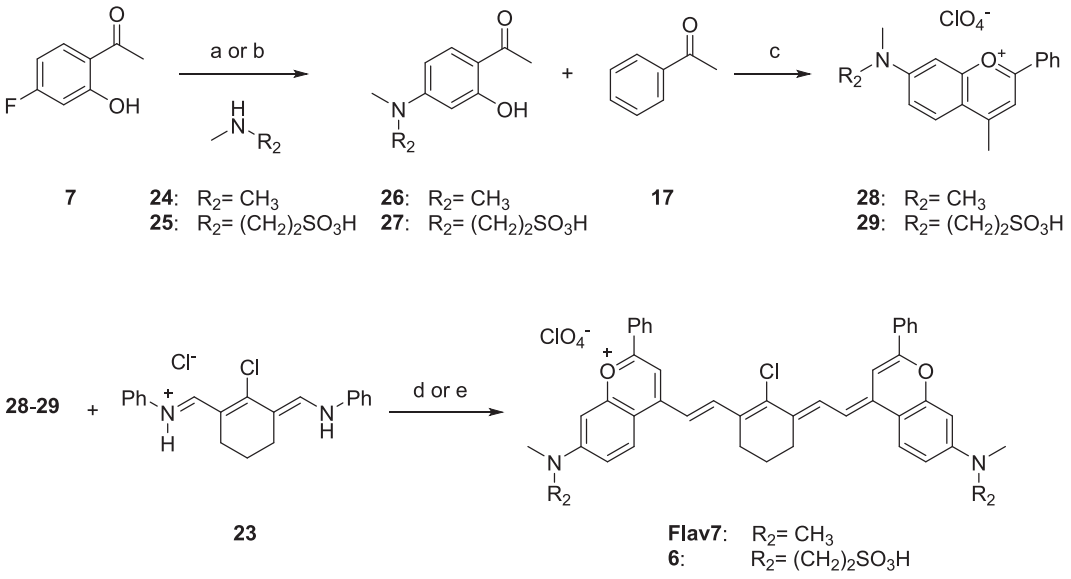

Scheme 2. Reagents and conditions: (a) 80 °C, 5 h, 83 %. (b) K_2CO_3, DMF, 110 °C, 24 h, 80 %. (c) $HClO_4$ 70 %, CH_3COOH, 105 °C, 20 h, 30–75 %. (d) NaOAc, *n*-BuOH/Toluene, 100 °C, 0.5 h, 30 %. (e) 2,6-di-*tert*-butyl-4-methylpyridine, *n*-BuOH/Toluene, 100 °C, 4 h, 7 %.

Absorption coefficients (ε) in dichloromethane were measured for all the newly synthesized compounds (Table 1). **FlavMorpho** (**1**) showed the highest value of molar extinction coefficient among the new derivatives of **Flav7**, while compound **2** exhibited the lowest value due to its limited absorption in DCM, in total agreement with the absorption spectra recorded. Interestingly, **FlavMorpho** (**1**) showed a higher fluorescence quantum yield (Φ_F) than **Flav7** in dichloromethane (Table 1) and an overall fluorescence brightness value ($\varepsilon_{max} \times \Phi_F$) similar to that of the parent compound **Flav7**.

Absorption and emission spectra were recorded in water as well. The shift of the main absorption peak towards shorter wavelengths, around 700–800 nm, became evident for all the newly synthesized compounds (Fig. 4A), while **Flav7** showed no significant absorption in water. However, despite the higher absorption of the new derivatives with respect to **Flav7**, water strongly quenched the fluorescence and no emission signals were collected for all the compounds, as for the parent compound (Fig. 4B). The hypsochromic shift in polar environments is usually correlated to the formation of aggregated forms, and more

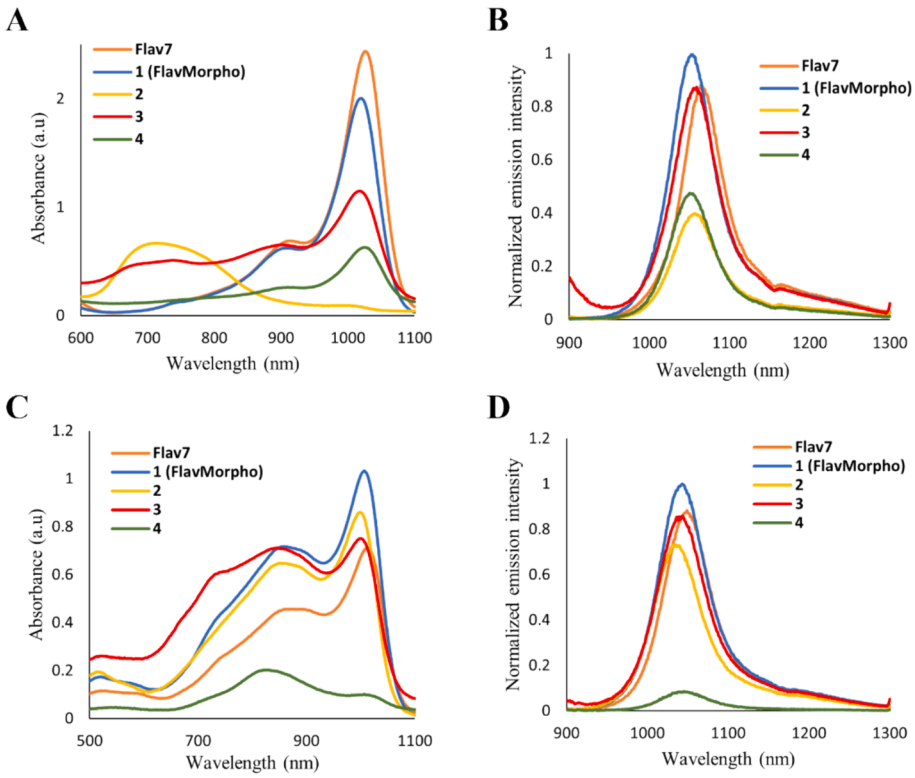

Fig. 3. Absorption (A) and normalized emission (B) spectra of compounds **1**–**4** and **Flav7** in dichloromethane (DCM). Absorption (C) and normalized emission (D) spectra of compounds **1**–**4** and **Flav7** in acetonitrile (ACN). Excitation wavelength λ = 870 nm.

Table 1
Photophysical properties of **Flav7** and compounds **1**–**4** in dichloromethane. Abbreviation: ND, not determined.

	$\lambda_{max,abs}$ (nm)	$\lambda_{max,em}$ (nm)	ε_{max} (M^{-1} cm^{-1})	Φ_F (%)	Brightness (M^{-1} cm^{-1})
Flav7	1027	1064	258 050	0.50 ± 0.05	1290
1 (FlavMorpho)	1020	1053	184 300	0.60 ± 0.05	1106
2	715	1056	7 175	ND	–
3	1018	1059	93 355	ND	–
4	1026	1050	13 281	ND	–

specifically to the formation of H-aggregates, that are known to cause a blue-shift in absorption [26]. The influence of the amount of water in altering the monomer – aggregate equilibrium was demonstrated by recording the absorption and emission spectra of all the compounds in mixtures containing increasing percentage of water in acetonitrile (Fig. S2). As the relative amount of water increased, the absorption of aggregate peak increased as well, and a specular reduction in emission intensity was detected. A peculiar behaviour was noted for compound **4** which showed a reduced formation of aggregates at low percentage of water (10–20 %) and a consequent higher emission. However, reaching 50 % water content, a marked decrease in emission intensity was observed. By directly comparing the emission of all the compounds in ACN with 10 % or 20 % water, **FlavMorpho** (**1**) proved to be the best emitter (Fig. S3).

To further assess whether the species absorbing at around 800 nm were aggregated forms generated by π-π stacking interactions, we investigated the aqueous behaviour of **FlavMorpho** (**1**). **FlavMorpho** (**1**) was analysed at lower concentrations (from 1 to 5 μM) in water (Fig. 4C, D). As the concentration of **1** increased, the absorption at shorter wavelengths became predominant. Since the formation of aggregates is a concentration-dependent phenomenon [30], it was possible to ascribe this absorption peak to aggregated forms. Under more concentrated conditions (20 μM), aggregation occurred massively for all new compounds and the monomer – aggregate equilibrium was completely shifted towards the latter form (Fig. 4A). By observing these data, we can infer that a different aggregation process occurred for new compounds compared to **Flav7**. While new polar compounds showed an absorption peak at shorter wavelengths, **Flav7** did not show any significant absorption in water (Fig. 4A). We can speculate that new derivatives behave as amphiphilic compounds, unlike **Flav7**, forming proper H-aggregates in water. These aggregates, partially solvated by water molecules on the newly introduced polar side of the scaffold, are maintained in suspension in polar environments thus giving detectable absorption. Conversely, **Flav7** may form aggregates that tend to precipitate in water, due to the compound's higher lipophilicity and the lower steric hindrance of the substituent group in position 7 of the scaffold, which may intensify π-π stacking interactions. This visually undetectable precipitation could therefore be responsible for the absence of absorption peaks. These data confirmed the increased polarity of the newly synthesized compounds compared to **Flav7**; however, the tendency to aggregate was not prevented for the new compounds too. In both cases, this aggregation tendency led to non-radiative decays, as confirmed by the absence of emission in pure water. Similar absorption and emission behaviour was observed analyzing compounds in phosphate buffered saline (PBS) solution at pH = 7.4 (Fig. S4).

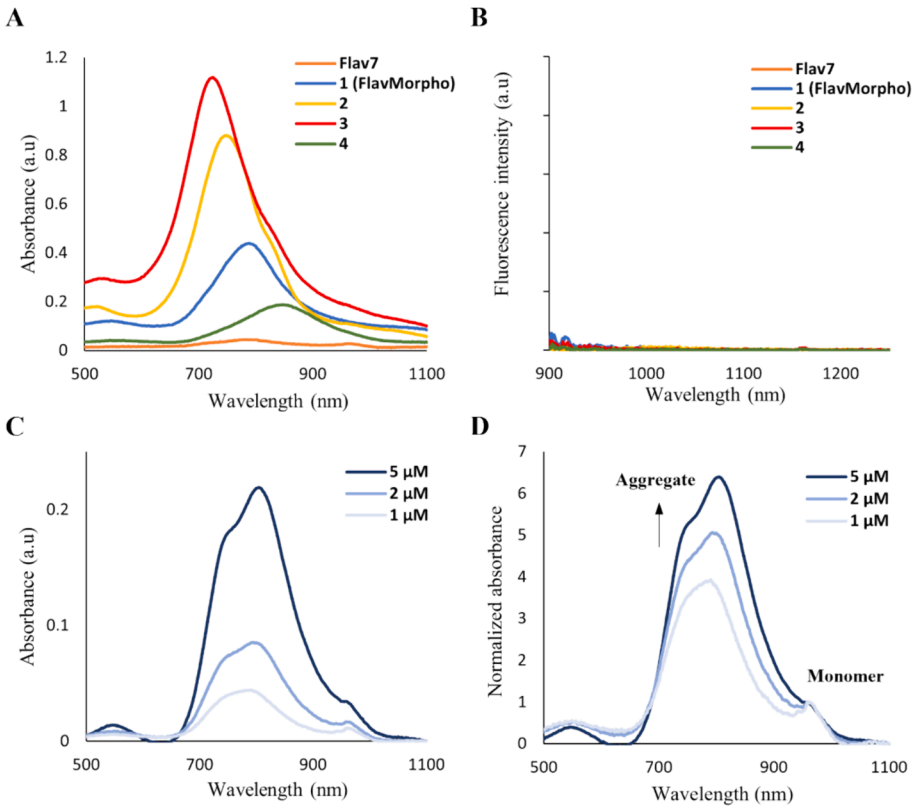

Fig. 4. Absorption (A) and emission (B) spectra of compounds **1**–**4** and **Flav7** (20 µM) in water. Excitation wavelength λ = 870 nm. Absorption (C) and normalized absorption (D) spectra of **FlavMorpho** (**1**) at increasing concentrations (1–2–5 µM) in water.

2.3. Stability in solution and monomer – aggregate equilibrium changes over time

Absorption spectra of **Flav7** and compounds **1**–**4** were continuously recorded over time, first to assess the stability in different polar media and then to evaluate whether changes in the equilibrium of monomer – aggregate forms were detectable. Compounds were analysed both in acetonitrile and in an acetonitrile/water (90:10) mixture at the same concentration of 20 µM. The variations in absorbance at the peak of the monomer form and the peak of the aggregate form as a function of time are shown in Fig. 5. Data were obtained by plotting the residual absorbance (%) measured at fixed time points against the absorbance measured at the starting point (t = 0 min), monitored at two different $\lambda_{max,abs}$, one of the monomer form (M peak) and one of the aggregated species (A peak, Fig. 5A) under the chosen solvent conditions. The wavelengths at which the absorbance variation over time was monitored were chosen for each compound in correspondence with the maximum absorption wavelength for the monomer form (around 1000 nm) and the local maximum of absorption at shorter wavelengths (around 840–890 nm) for the aggregate species and are reported in Fig. S5. Variations of absorption spectra of all compounds over time are also available in Fig. S5.

Flav7, **FlavMorpho** (**1**) and compound **2** proved to be stable in acetonitrile, with minimal changes in absorption over time (Fig. 5B-D). In presence of 10 % water in acetonitrile, **Flav7** and compound **2** showed a significant reduction of absorption over time, with a residual absorbance of about 80 % after 3 h. **FlavMorpho** (**1**), instead, showed good stability even under these conditions, with a residual absorbance >90 % after 3 h. For all these compounds, the variation in absorption at the monomer peak (M) was accompanied by the same variation at the aggregate peak (A), meaning that the monomer – aggregate equilibrium was not affected over time. The reduction in absorbance could most likely be attributed to a photodegradation process, which occurs for both monomers and aggregates. Interestingly, compounds **3** and **4** showed a different behaviour. Over time, compound **3** exhibited an increasing absorbance in acetonitrile, that was observed for both the monomer (Fig. 5E, blue line ACN (M)) and the aggregate peak (Fig. 5E, light-blue line ACN (A)). This behaviour, which can be explained by a gradual increment in concentration, could be attributed to an increasing dissolution of the compound in acetonitrile over time, although visual inspection of the solution of **3** did not show undissolved material at the beginning of the experiment. In the presence of 10 % water in acetonitrile, this behaviour was no longer detected, and a slight reduction in absorption over time was observed, similar to **FlavMorpho** (**1**). Differently from the previous compounds, product **4** showed indeed a variation in the monomer – aggregate equilibrium over time (Fig. 5F). While the monomer peak increased with time, that of the aggregate slowly decreased. The shift towards the monomeric form was detected both in acetonitrile alone and in the presence of 10 % water. The reasons for this behaviour are still to be clarified. The substantial difference of compound **4** from the others is the presence of two negatively charged substituent groups on the scaffold, which may play a specific role in the aggregation – disaggregation process.

Overall, the optical properties of **FlavMorpho** (**1**) as well as its higher stability in different conditions led us to choose this compound for further investigations.

2.4. Micelles formulation and characterization

In view of possible applications in biological settings, **FlavMorpho** (**1**) and **Flav7** were encapsulated in phospholipidic micelles to increase their water solubility. Dyes were loaded into micelles with varying loading capacities of 4 %, 2 % and 1 % weight, and all micelles in PBS (pH 7.4) were characterized by dynamic light scattering (DLS) analysis. Consistently, by increasing the amount of loaded fluorophore, micelles dimensions increased, while maintaining proper nanometric sizes

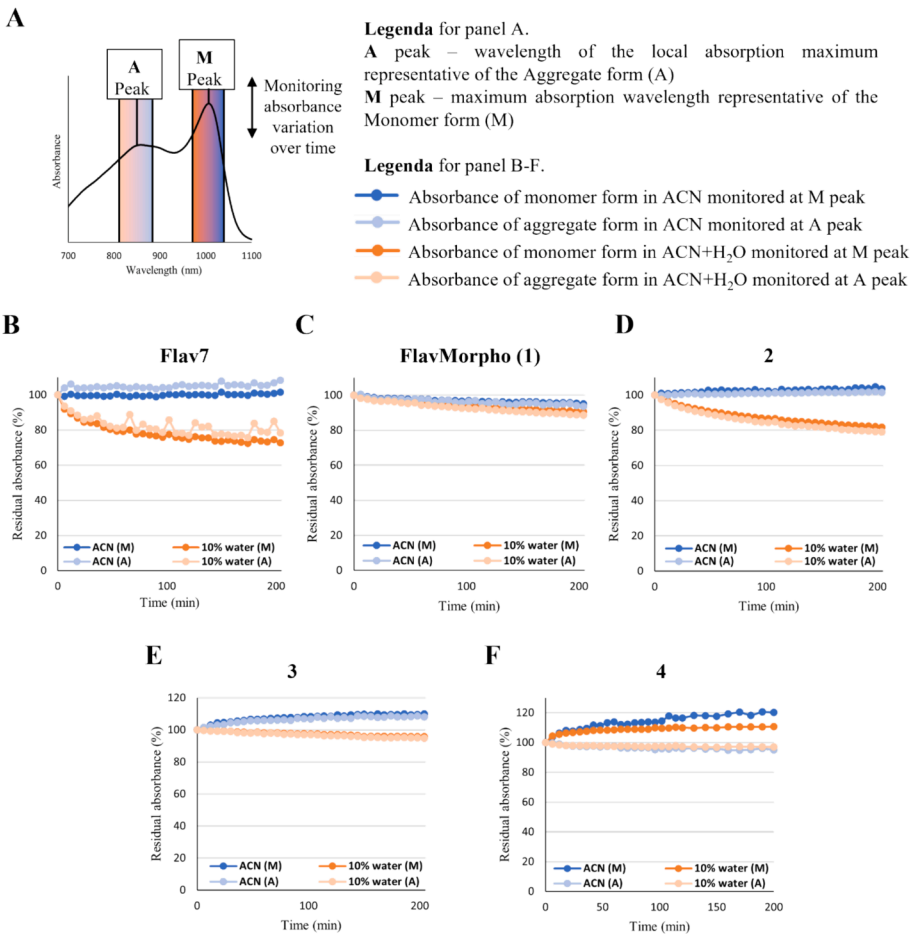

Fig. 5. (A) Schematic representation of the monitored peaks. Residual absorbance (%) over time monitored at $\lambda_{max,abs}$ of monomer form and at $\lambda_{max,abs}$ of aggregates in acetonitrile and acetonitrile/water 90:10 of **Flav7** (B), **FlavMorpho** (**1**) (C) and compounds **2** (D), **3** (E) and **4** (F). See Legenda for panel B-F in the figure.

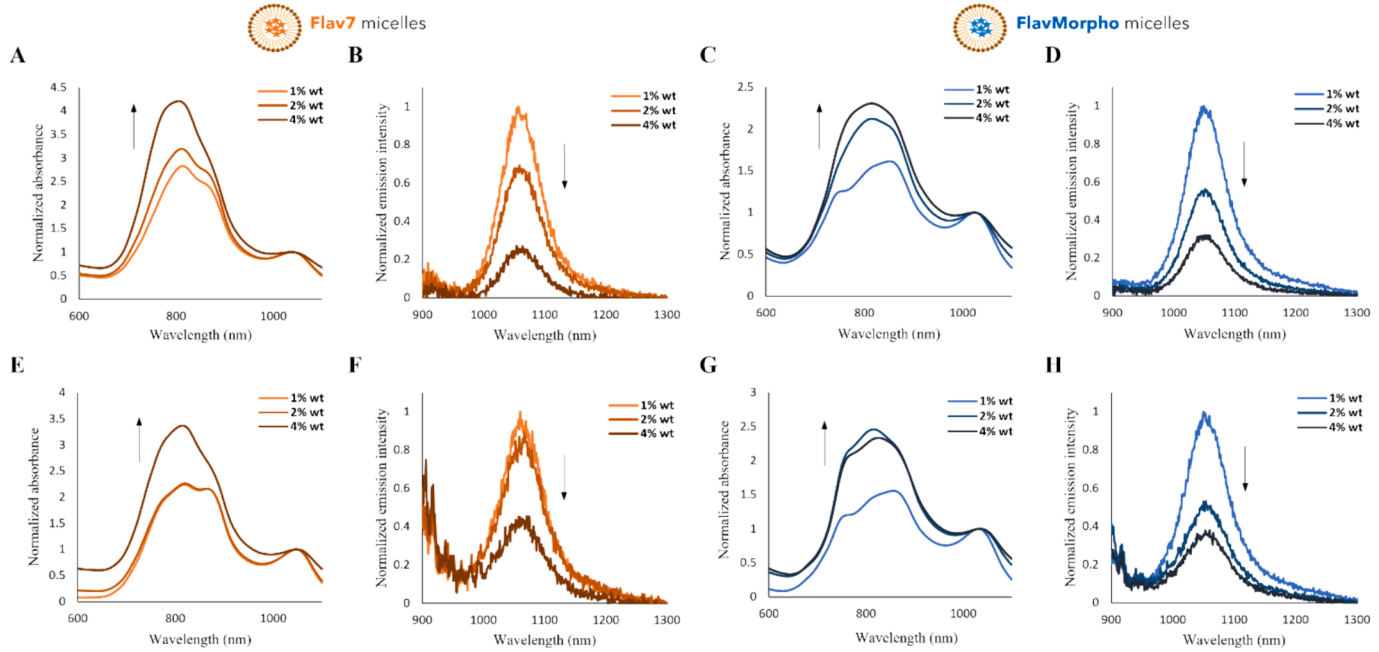

Fig. 6. Normalized absorption and emission spectra in PBS of **Flav7** micelles (A, B) and **FlavMorpho** (**1**) micelles (C, D) at different loading capacities. Normalized absorption and emission spectra in serum of **Flav7** micelles (E, F) and **FlavMorpho** (**1**) micelles (G, H) at different loading capacities. Excitation wavelength $\lambda = 870$ nm. Arrows indicate the shifting trend of the spectra at the aggregate peak in the absorption spectra and of emission intensity in the emission spectra as the amount of loaded fluorophore increases.

Table 2
Z-average and polydispersity index (PDI) values for differently loaded micelles measured by DLS analysis, and respective concentrations of the encapsulated fluorophore. [a] Interpolated from a standard curve.

Loaded fluorophore	*Micelle loading*	*Z-average (d. nm)*	*PDI*	*Concentration (μM)[a]*
Flav7	1 % wt	14.85	0.220	45.5
	2 % wt	18.23	0.305	69.0
	4 % wt	37.09	0.527	160.5
FlavMorpho (1)	1 % wt	15.95	0.296	40.2
	2 % wt	17.85	0.319	88.4
	4 % wt	32.77	0.538	121.1
Empty micelles		12.76	0.101	

(Table 2 and Fig. S6 A-G). Phospholipidic micelles proved to be stable for more than one month when stored at 4 °C in PBS, as dimensions were unaltered after DLS analysis (Fig. S6 H-I). The actual fluorophore concentrations for each type of differently loaded micelles were spectrophotometrically quantified (Table 2), and optical characterization was performed for all micelles at the same final concentration of 20 μM in PBS and serum (Fig. 6A-H).

Through encapsulation in micelles, both the compounds emit in the SWIR region in aqueous environments such as PBS and serum (Fig. 6B, D, F, H). As the amount of loaded fluorophore increased, evident aggregation phenomena occurred within the micelles in both tested solvents, as visible from the increase in absorbance of the aggregate peak in the absorption spectra of both compounds. These aggregation phenomena are again responsible for aggregation-caused quenching (ACQ) effect and the concomitant reduction in emission intensity with increasing fluorophore loading, as visible from the emission spectra of both compounds in both tested solvents. Micelles loaded with the lowest amount of fluorophore (1 % wt) resulted in the best formulation for both compounds. Furthermore, when directly comparing **FlavMorpho (1)** and **Flav7** micelles 1 % wt, **FlavMorpho (1)** micelles 1 % wt showed an emission intensity twice as high as **Flav7** micelles 1 % wt in both PBS and serum (Fig. 7), thus emerging as a better SWIR emitter in aqueous media.

2.5. SWIR emission assessment and brightness comparison

Dye-loaded micelles were also studied in comparison with the reference cyanine compound indocyanine green (**ICG**), to evaluate the extent of SWIR emission of the different dyes. As recently reported, ICG can not only be used as NIR-I emitter, but it also exhibits tail-emission in the SWIR region [31–34]. Since ICG was the first FDA-approved fluorophore, most of the devices used for optical imaging were built supporting the most suitable excitation wavelength for ICG (λ = 805/808 nm). We therefore collected and compared the emission in the SWIR region (1040–1400 nm) of the three fluorophores (**ICG**, **Flav7** micelles 1 % wt and **FlavMorpho (1)** micelles 1 % wt) in PBS and serum, using the same excitation wavelength (λ = 808 nm) and analyzing the compounds at the same concentration of 2 μM (Fig. 8). At this sub-optimal excitation wavelength, both **FlavMorpho** and **Flav7** micelles revealed a significantly lower emission intensity compared to **ICG**, for which the excitation wavelength was the most suitable, both in PBS (Fig. 8A) and, especially, in serum (Fig. 8B). However, even under these unfavorable conditions, **FlavMorpho** showed a higher emission intensity compared to **Flav7**, as also confirmed by the so-obtained Area Under the Curve (AUC) values (Table 3). It is noteworthy that, when all the dyes were excited at their respective maximum absorption wavelength in PBS (Fig. 8C), **FlavMorpho (1)** showed an emission intensity twice as high as **Flav7** in the SWIR region and, more importantly, almost five times higher than the reference **ICG**. Nonetheless, **ICG** remains the most emissive dye in serum even when exciting all fluorophores at their maximum of absorption (Fig. 8D), albeit with an AUC value not excessively different from those shown by **FlavMorpho (1)** and **Flav7** micelles (Table 3). However, it should be emphasized that the use of an excitation wavelength in the SWIR region could offer some advantages over the excitation in the NIR-I region, such as better resolution, greater penetration depth and also a higher maximum permissible exposure (MPE) to laser [35,36].

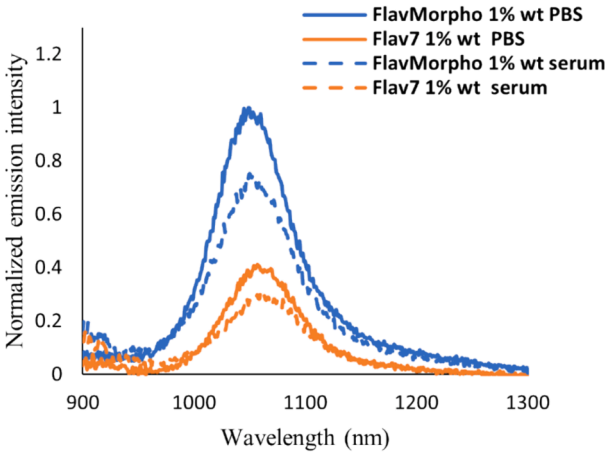

Fig. 7. Direct comparison of normalized emission spectra of **FlavMorpho (1)** micelles 1% wt and **Flav7** micelles 1% wt in PBS (solid lines) and serum (dashed lines).

These results give credit to the fact that the availability of fine-tuned lasers at different wavelengths, supported by modern or to-be-developed optical imaging devices, could significantly improve and enhance the SWIR application of these flavylium-based fluorophores.

Finally, the SWIR brightness of **FlavMorpho (1)** and **Flav7** micelles was checked using a prototype SWIR imaging device. Micelles over a range of concentrations in PBS and serum were irradiated with 808 nm light and the emission was revealed with an InGaAs camera using a 1100-nm long-pass filter and an exposure time of 150 ms. **FlavMorpho (1)** confirmed the improved optical properties compared to **Flav7**, showing a higher detectable brightness and a lower limit of detection (LOD) of 0.5 μM in PBS (Fig. 9), and showed a similar behaviour to **Flav7** when analyzed in serum (Fig. S7). Since these results confirmed previously collected data, we are prone to believe that having a SWIR device supported with an adjusted excitation wavelength, capable of exciting the dyes around or at their maximum absorption wavelength, may result in significantly implemented SWIR imaging of these fluorophores.

3. Conclusion

Chemical modulation of the dimethylamino group of **Flav7** with different cyclic or linear amino groups, chosen to increase the polarity of the fluorophores, furnished a series of new SWIR emitters. The development of a new and versatile synthetic procedure constituted a significant tool for the obtainment of all the designed compounds. Newly developed compounds shared the favourable optical profile in organic solvents as the parent compound, with derivative **FlavMorpho (1)** being even more emissive compared to **Flav7** in different solvents. In polar environments, all the new compounds still exhibited a tendency to aggregate, which was reflected in an absence of fluorescence emission in water. However, aggregates generated by new products were able to remain suspended in water and act as H-aggregates due to the amphiphilic and more polar character of compounds, whereas the **Flav7** aggregates most likely precipitated, with a complete loss of absorption, due to the higher lipophilicity. We also found that the monomer – aggregate equilibrium in polar solvents such as acetonitrile and acetonitrile/water 90:10 can change and shift towards one form rather than

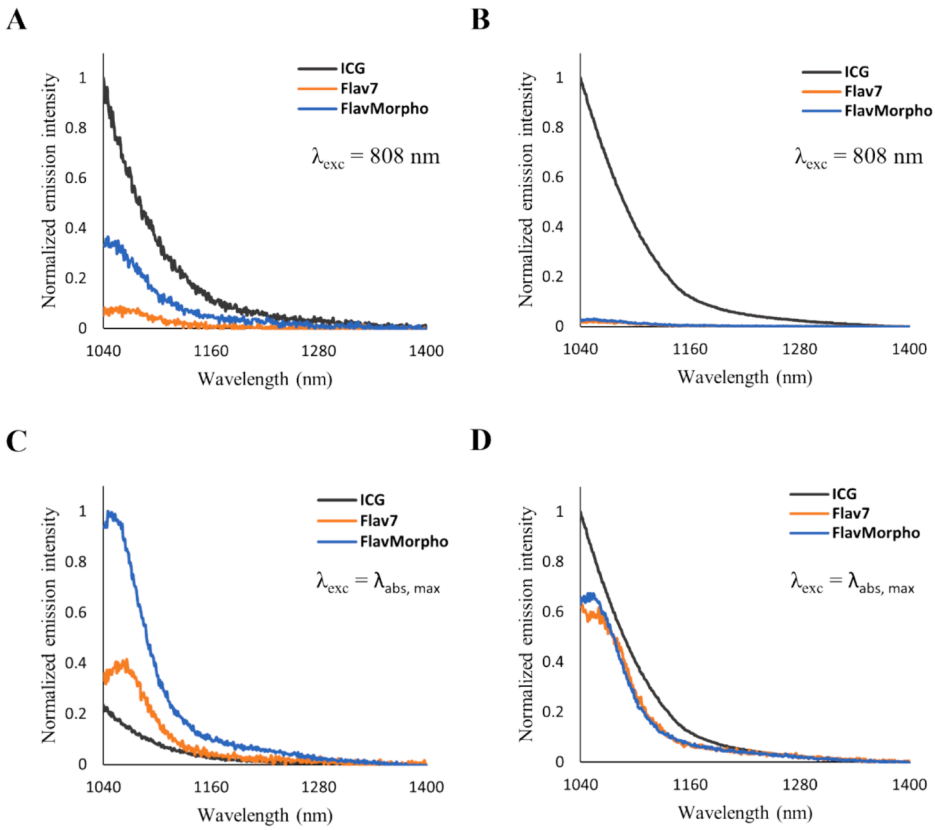

Fig. 8. (A, B) Normalized emission spectra of **ICG**, **Flav7** micelles 1 % wt and **FlavMorpho** (**1**) micelles 1 % wt in the SWIR range (1040–1400 nm) using as excitation wavelength λ = 808 nm in PBS (A) and in serum (B). (C, D) Normalized emission spectra of **ICG**, **Flav7** micelles 1 % wt and **FlavMorpho** (**1**) micelles 1 % wt in the SWIR range (1040–1400 nm) using as excitation wavelength the respective maximum absorption wavelength for each compound (λ = 808 nm for **ICG**; λ = 1012 nm for **FlavMorpho** (**1**) micelles 1 % wt; λ = 1019 nm for **Flav7** micelles 1 % wt) in PBS (C) and in serum (D).

Table 3
Extent of SWIR emission. [a]Integral value of the emission between 1040 and 1400 nm, exciting the dyes at the reported wavelength and in the corresponding solvent.

Compound	*Excitation wavelength (nm)*	*AUC (1040–1400 nm)* [a]	
		PBS	*Serum*
ICG	808	10.0×10^5	92.3×10^5
Flav7	808	0.88×10^5	2.51×10^5
	1019	20.2×10^5	65.6×10^5
FlavMorpho (1)	808	4.19×10^5	3.61×10^5
	1012	46.5×10^5	66.4×10^5

another over time for some compounds. Further in-depth analysis of this behaviour might reveal different uses for these fluorophores.

Very recently, when this manuscript was in preparation, a paper was published in which the same aim of modifying the Flav7 scaffold to obtain water-soluble derivatives was pursued [37]. Soluble compounds with improved optical properties have been obtained by derivatizing the flavylium scaffold with sulfonates or ammonium groups, which are connected to the electron-donating amino group via a fairly long linker containing a triazole ring generated by click reaction. Evidently, the building of a scaffold bearing multiple permanent charges contributes significantly to increase water solubility. Moreover, the elevated ramification and substitution of the recently reported derivatives, may also play a role in shielding not only the π-conjugated scaffold from other molecules, thus avoiding π-π stacking interactions, but also the lipophilic part of the molecule from the surrounding aqueous media, thus limiting the tendency to aggregate and allowing fluorescence emission.

Adopting another strategy to impart water solubility as nanocarrier encapsulation, we developed phospholipidic micelles of **FlavMorpho** (**1**) and **Flav7**. When formulated in micelles, both compounds revealed SWIR absorption and emission in polar media such as PBS (pH 7.4) and serum, with **FlavMorpho** (**1**) being twice as emissive as the parent compound. The comparison of **FlavMorpho** (**1**) and **Flav7** micelles with **ICG** in terms of emission in the SWIR region in PBS revealed that, by exciting the dyes at their respective absorption maxima, **FlavMorpho** (**1**) possesses a higher SWIR emission extent not only than **Flav7**, but, more importantly, than the reference **ICG**. The availability of optical imaging devices equipped with fine-tuned lasers, capable of exciting these dyes at their maximum of absorption in the NIR-II region, may lead to significantly implemented SWIR imaging results and could pave the way for a more effective imaging technique and for fluorescence-guided surgical applications.

4. Experimental section

4.1. Materials and instruments

Unless otherwise noted, all commercial reagents and solvents were purchased from commercial suppliers and used without further purification. Tetrahydrofuran (THF) was freshly distilled from sodium wires/benzophenone under nitrogen atmosphere. Dry toluene was either purchased or distilled from sodium under nitrogen atmosphere. Dry *n*-butanol was purchased and stored over 3 Å molecular sieves. All air and moisture sensitive reactions were carried out in flame-dried glassware under a nitrogen atmosphere. All the reactions were monitored by thin layer chromatography (TLC) on Merck 60 F254 (0.25 mm) plates, which were visualized by UV inspection (254 nm). Flash chromatography purifications were performed using silica gel Merck with 60 mesh particles.

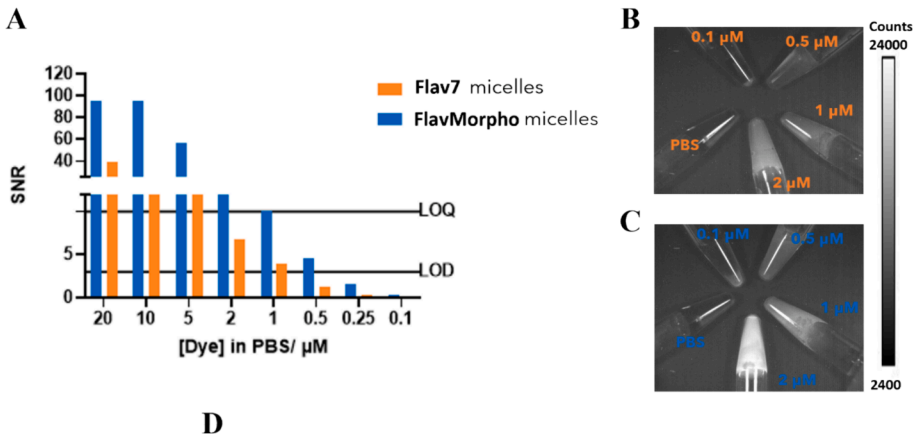

D

Dye	LOD/[µM]	LOQ/[µM]
Flav7	1	5.0
FlavMorpho	0.5	1.0

Fig. 9. (A) Signal-to-noise ratio of **Flav7** and **FlavMorpho** (**1**) micelles 1% wt at different concentrations when imaged with SWIR device. Visual representation of the differently concentrated solutions of **Flav7** micelles (B) and **FlavMorpho** (**1**) micelles (C) imaged through SWIR imaging device. (D) Limit of Detection (LOD) and Limit of Quantification (LOQ) values of **Flav7** and **FlavMorpho** (**1**) micelles 1% wt.

ESI-mass spectra were recorded on a Waters Micromass Quattro Micro equipped with an ESI source. High-resolution mass spectra (HRMS) were obtained with a micrOTOF (Bruker Daltonics). High-performance liquid chromatography (HPLC) analyses were performed with a Agilent 1200 system, using a Poroshell EC-C18 column (100 × 4.6 mm, 2.7 µm). Semi-preparative HPLC separation was carried out on a HPLC-MS (Agilent mod. 1260, Quadrupole LC/MS Mod. 6120) equipped with an UV–Vis absorption detector set at different wavelengths and a Gemini NX-C18 column (250 × 10 mm, 5 µm). The purity of the final compounds was determined by RP-HPLC and performed with the same instruments. ^{1}H and ^{13}C NMR spectra were registered on JEOL ECZR600 spectrometer, at 600 and 151 MHz, respectively. Coupling constants (J) are given in Hertz (Hz) and chemical shifts (δ) are given in ppm, calibrated to solvent signal as internal standard. Following abbreviations are used to describe multiplicities: s = singlet, d = doublet, t = triplet, q = quadruplet, m = multiplet, br = broad and dd = doublet of doublet. The absorption spectra were recorded with a Perkin Elmer Lambda 365 UV–VIS spectrophotometer, with acquisition range of 500–1100 nm. The emission spectra were recorded with a FluoroLog-3 1IHR-320 spectrofluorometer with 450 W Xenon Light source. Detection was performed by near infrared photomultiplier tubes (PMT-NIR, R5509) cooled detector, with acquisition range 900–1300 nm for NIR-II emission. Nanomaterial size was analyzed with a Zetasizer NanoZS (Malvern) in plastic 1 cm cuvettes.

4.2. 1-(2-hydroxy-4-morpholinophenyl)ethan-1-one (12)

In a round-bottom flask, 1-(4-fluoro-2-hydroxyphenyl)ethan-1-one (**7**, 1 g, 6.49 mmol, 1 eq) and morpholine (**8**, 5.6 mL, 64.9 mmol, 10 eq) were mixed and stirred at 120 °C for 1 h. The mixture was then cooled to RT, diluted with water and extracted with AcOEt (3 × 20 mL). The combined organic phases were dried over Na_2SO_4 and concentrated under reduced pressure. The crude product was purified by silica gel chromatography (PE/AcOEt 8:2) to afford product **12** (1.29 g, 90 % yield) as a white solid. ^{1}H NMR (600 MHz, $CDCl_3$) δ 12.72 (s, 1H), 7.57 (d, J = 9.0 Hz, 1H), 6.39 (dd, J = 9.0, 2.4 Hz, 1H), 6.28 (d, J = 2.4 Hz, 1H), 3.83 (t, J = 5.0 Hz, 4H), 3.32 (t, J = 5.0 Hz, 4H), 2.51 (s, 3H). ^{13}C NMR (151 MHz, $CDCl_3$) δ 201.5, 164.7, 156.4, 132.3, 112.1, 105.4, 100.5, 66.4, 47.0, 25.8. MS (ESI^+): m/z 222.4 $[M + H]^+$.

4.3. 1-(2-hydroxy-4-(4-methylpiperazin-1-yl)phenyl)ethan-1-one (13)

In a screw-capped vial, compound **7** (200 mg, 1.30 mmol, 1 eq) and *N*-methylpiperazine (**9**, 0.4 mL, 3.89 mmol, 3 eq) were mixed and stirred at 130 °C for 2 h. The mixture was directly loaded onto a silica gel column and purified (DCM/MeOH gradient mode from 99:1 to 97:3) to give **13** (253 mg, 83 % yield) as a yellowish solid. ^{1}H NMR (600 MHz, $CDCl_3$) δ 12.74 (s, 1H), 7.53 (d, J = 9.3 Hz, 1H), 6.37 (dd, J = 9.1, 2.6 Hz, 1H), 6.26 (d, J = 2.8 Hz, 1H), 3.37 (t, J = 5.2 Hz, 4H), 2.50 (t, J = 5.2 Hz, 4H), 2.49 (s, 3H), 2.32 (s, 3H). ^{13}C NMR (151 MHz, $CDCl_3$) δ 201.2, 164.8, 156.3, 132.2, 111.5, 105.5, 100.2, 54.6, 46.7, 46.1, 25.7. MS (ESI^+): m/z 235.5 $[M + H]^+$.

4.4. Ethyl 1-(4-acetyl-3-hydroxyphenyl)piperidine-4-carboxylate (14)

In a round-bottom flask, compound **7** (200 mg, 1.30 mmol, 1 eq) and ethyl piperidine-4-carboxylate (**10**, 2 mL, 13.0 mmol, 10 eq) were mixed and stirred at 120 °C for 3 h. The mixture was then cooled to RT, diluted with water and extracted with DCM (3 × 20 mL). The combined organic phases were dried over Na_2SO_4 and concentrated under reduced pressure. The crude product was purified by silica gel chromatography (PE/AcOEt gradient mode from 9:1 to 85:15) to afford **14** (250 mg, 66 % yield) as a whitish solid. ^{1}H NMR (600 MHz, $CDCl_3$) δ 12.75 (s, 1H), 7.53 (d, J = 9.0 Hz, 1H), 6.37 (dd, J = 9.1, 2.6 Hz, 1H), 6.26 (d, J = 2.4 Hz, 1H), 4.15 (q, J = 7.1 Hz, 2H), 3.84 (dt, J = 13.4, 3.8 Hz, 2H), 3.03–2.98 (m, 2H), 2.57–2.52 (m, 1H), 2.49 (s, 3H), 1.98 (dd, J = 13.6, 3.6 Hz, 2H), 1.79 (m, 2H), 1.26 (t, J = 7.1 Hz, 3H). ^{13}C NMR (151 MHz, $CDCl_3$) δ 201.0, 174.3, 164.9, 156.0, 132.3, 111.2, 105.7, 100.2, 60.6, 46.6, 40.9, 27.4, 25.7, 14.2. MS (ESI^+): m/z 314.2 $[M + Na]^+$.

4.5. 1-(2-hydroxy-4-(piperazin-1-yl)phenyl)ethan-1-one (15)

To a solution of piperazine **11** (503 mg, 5.84 mmol, 3 eq) in DMSO (9 mL), compound **7** (300 mg, 1.95 mmol, 1 eq) was added under nitrogen and the reaction was stirred at 110 °C for 2 h. The mixture was cooled to RT, diluted with water and extracted with AcOEt (7 × 20 mL). The combined organic phases were washed with brine (40 mL), dried over Na_2SO_4, and concentrated under reduced pressure. The crude product was purified by silica gel chromatography (DCM/MeOH + NH_3 98:2) to give **15** (347 mg, 81 % yield) as a yellow solid. ^{1}H NMR (600 MHz, $CDCl_3$) δ 12.75 (s, 1H), 7.53 (d, J = 9.0 Hz, 1H), 6.36 (dd, J = 9.1,

2.6 Hz, 1H), 6.25 (d, $J = 2.4$ Hz, 1H), 3.32 (t, $J = 5.0$ Hz, 4H), 2.97 (t, $J = 5.2$ Hz, 4H), 2.60 (s, 1H), 2.49 (s, 3H). ^{13}C NMR (151 MHz, $CDCl_3$) δ 201.2, 164.8, 156.6, 132.2, 111.5, 105.5, 100.1, 47.8, 45.7, 25.7. MS (ESI^+): *m/z* 221.5 $[M + H]^+$.

4.6. 4-(4-(4-acetyl-3-hydroxyphenyl)piperazin-1-yl)butane-1-sulfonic acid (16)

Compound **15** (100 mg, 0.45 mmol, 1 eq) was dissolved in 1,4-dioxane (2 mL) and 1,4-butansultone (464 μL, 4.54 mmol, 10 eq) was added dropwise. The mixture was stirred at 95 °C for 24 h. Other 1,4-butansultone (232 μL, 2.27 mmol, 5 eq) was added and the reaction was maintained under stirring for another 6 h, then a precipitate was formed. The mixture was cooled to RT, the precipitate was filtered, washed with 1,4-dioxane, and dried under vacuum to afford compound **16** (145 mg, 89 % yield) as a greyish solid, which was used in the following step without further purification. ^{1}H NMR (600 MHz, DMSO-d_6) δ 12.70 (s, 1H), 7.74 (d, $J = 8.6$ Hz, 1H), 6.59 (d, $J = 8.6$ Hz, 1H), 6.39 (s, 1H), 4.11 (d, $J = 6.5$ Hz, 2H), 3.55–3.46 (m, 2H), 3.34–3.40 (m, 2H), 3.20–3.14 (m, 4H), 3.04 (s, 3H), 2.50–2.53 (m, 2H), 1.77 (br, 2H), 1.62 (t, $J = 6.7$ Hz, 2H). MS (ESI^+): *m/z* 379.4 $[M + Na]^+$.

4.7. 4-methyl-7-morpholino-2-phenylchromenylium perchlorate (18)

Compound **12** (500 mg, 2.26 mmol, 1 eq) and acetophenone **17** (1.2 mL, 10.4 mmol, 4.6 eq) were dissolved in acetic acid (8.7 mL), and perchloric acid 70 % (4.4 mL) was added dropwise at room temperature. The reaction was stirred at 105 °C for 20 h under a nitrogen atmosphere. After being cooled to room temperature, water was added to the mixture to facilitate a dark red precipitate. The precipitate was filtered, washed with diethyl ether, and dried under vacuum to obtain compound **18** (639 mg, 70 % yield) which was used in the following step without further purification. ^{1}H NMR (600 MHz, Acetonitrile-d_3) δ 8.31–8.28 (m, 2H), 8.22–8.17 (m, 1H), 8.03–8.00 (m, 1H), 7.79–7.76 (m, 1H), 7.71–7.68 (m, 2H), 7.62–7.59 (m, 1H), 7.50 (d, $J = 10.3$ Hz, 1H), 3.90–3.86 (m, 4H), 3.78–3.74 (m, 4H), 2.92–2.88 (m, 3H). ^{13}C NMR (151 MHz, Acetonitrile-d_3) δ 167.3, 165.9, 159.7, 157.0, 136.1, 130.9, 130.4, 130.1, 129.3, 120.5, 119.9, 115.0, 100.8, 66.5, 49.6, 20.6. MS (ESI^+): *m/z* 306.4 $[M]^+$.

4.8. 4-methyl-7-(4-methylpiperazin-1-yl)-2-phenylchromenylium perchlorate (19)

Compound **13** (230 mg, 0.98 mmol, 1 eq) and acetophenone **17** (458 μL, 3.93 mmol, 4 eq) were dissolved in acetic acid (4 mL), and perchloric acid 70 % (2 mL) was added dropwise at room temperature. The reaction was stirred at 105 °C for 20 h under a nitrogen atmosphere. After being cooled to room temperature, ethyl acetate was added to the mixture to facilitate an orange-red precipitate. The precipitate was filtered, washed with diethyl ether, and dried under vacuum to obtain compound **19** (208 mg, 51 % yield) which was used in the following step without further purification. ^{1}H NMR (600 MHz, DMSO-d_6) δ 8.43 (s, 1H), 8.38 (d, $J = 8.6$ Hz, 2H), 8.33 (d, $J = 10.1$ Hz, 1H), 7.82–7.80 (m, 2H), 7.76–7.73 (m, 2H), 7.72 (s, 1H), 3.64 (d, $J = 12.3$ Hz, 2H), 3.21 (d, $J = 10.7$ Hz, 2H), 3.15–3.01 (m, 2H), 2.96 (s, 3H), 2.88 (s, 3H), 2.86 (d, $J = 4.5$ Hz, 2H). ^{13}C NMR (151 MHz, DMSO-d_6) δ 166.4, 163.3, 163.3, 158.6, 134.8, 129.8, 129.8, 129.3, 128.1, 124.3, 118.5, 113.5, 98.2, 51.9, 44.0, 42.1, 20.0. MS (ESI^+): *m/z* 319.4 $[M]^+$.

4.9. 7-(4-carboxypiperidin-1-yl)-4-methyl-2-phenylchromenylium perchlorate (20)

Compound **14** (100 mg, 0.34 mmol, 1 eq) and acetophenone **17** (184 μL, 1.58 mmol, 4.6 eq) were dissolved in acetic acid (2 mL), and perchloric acid 70 % (1 mL) was added dropwise at room temperature. The reaction was stirred at 105 °C for 24 h under a nitrogen atmosphere. After being cooled to room temperature, water was added to the mixture to facilitate a violet-black precipitate. The precipitate was filtered, washed with diethyl ether, and dried under vacuum to obtain compound **20** (97 mg, 63 % yield) which was used in the following step without further purification. ^{1}H NMR (600 MHz, CD_3OD) δ 8.32 (d, $J = 7.6$ Hz, 2H), 8.17 (d, $J = 10.0$ Hz, 1H), 8.01 (s, 1H), 7.73 (d, $J = 7.6$ Hz, 1H), 7.67 (t, $J = 7.7$ Hz, 2H), 7.64 (dd, $J = 9.6$, 2.4 Hz, 1H), 7.45 (d, $J = 2.4$ Hz, 1H), 4.33 (dd, $J = 10.3$, 3.4 Hz, 2H), 3.52–3.48 (m, 2H), 2.90 (s, 3H), 2.84–2.79 (m, 1H), 2.15 (dd, $J = 13.8$, 3.8 Hz, 2H), 1.87–1.81 (m, 2H). ^{13}C NMR (151 MHz, CD_3OD) δ 177.3, 160.8, 158.4, 155.6, 139.2, 135.2, 130.8, 130.7, 130.0, 128.8, 119.6, 119.4, 113.3, 97.9, 41.1, 29.0, 28.9, 17.1. MS (ESI^+): *m/z* 348.29 $[M]^+$.

4.10. 4-methyl-2-phenyl-7-(piperazin-1-yl)chromenylium perchlorate (21)

Compound **15** (345 mg, 1.57 mmol, 1 eq) and acetophenone **17** (731 μL, 6.27 mmol, 4 eq) were dissolved in acetic acid (7 mL), and perchloric acid 70 % (3.5 mL) was added dropwise at room temperature. The reaction was stirred at 105 °C for 20 h under a nitrogen atmosphere. After being cooled to room temperature, water was added to the mixture to facilitate an orange-red precipitate. The precipitate was filtered, washed with diethyl ether, and dried under vacuum to obtain compound **21** (360 mg, 57 % yield) which was used in the following step without further purification. ^{1}H NMR (600 MHz, CD_3OD) δ 8.38 (d, $J = 8.6$ Hz, 2H), 8.29 (d, $J = 9.6$ Hz, 1H), 8.22 (s, 1H), 7.77 (t, $J = 7.4$ Hz, 1H), 7.70–7.69 (m, 2H), 7.68 (d, $J = 2.8$ Hz, 1H), 7.61 (d, $J = 2.4$ Hz, 1H), 4.08 (t, $J = 5.3$ Hz, 4H), 3.46 (t, $J = 5.2$ Hz, 4H), 2.99–2.96 (m, 2H). {peak at 2.99–2.96 appears as a multiplet and as <3H due to proton-deuterium exchange with Methanol-d_4}. ^{13}C NMR (151 MHz, DMSO-d_6) δ 166.0, 165.9, 156.8, 139.3, 134.7, 129.8, 129.3, 129.2, 128.1, 118.5, 118.1, 113.4, 97.9, 43.9, 42.4, 19.9. MS (ESI^+): *m/z* 305.5 $[M]^+$.

4.11. 4-methyl-2-phenyl-7-(4-(4-sulfobutyl)piperazin-1-yl) chromenylium perchlorate (22)

Compound **16** (120 mg, 0.34 mmol, 1 eq) and acetophenone **17** (181 μL, 1.55 mmol, 4.6 eq) were dissolved in acetic acid (2.2 mL), and perchloric acid 70 % (1.1 mL) was added dropwise at room temperature. The reaction was stirred at 105 °C for 20 h under a nitrogen atmosphere. After being cooled to room temperature, ethyl acetate was added to the mixture to facilitate an orange-red precipitate. The precipitate was filtered, washed with diethyl ether, and dried under vacuum to obtain compound **22** (55 mg, 30 % yield) which was used in the following step without further purification. ^{1}H NMR (600 MHz, DMSO-d_6) δ 8.42 (s, 1H), 8.39 (d, $J = 7.6$ Hz, 2H), 8.32 (d, $J = 10.0$ Hz, 1H), 7.81 (t, $J = 7.4$ Hz, 1H), 7.75–7.73 (m, 4H), 4.56 (d, $J = 14.1$ Hz, 2H), 3.69 (d, $J = 11.7$ Hz, 2H), 3.57 (t, $J = 12.7$ Hz, 2H), 3.19 (d, $J = 8.3$ Hz, 4H), 2.95 (s, 3H), 2.54 (t, $J = 7.2$ Hz, 2H), 1.85–1.80 (m, 2H), 1.69–1.64 (m, 2H). MS (ESI^+): *m/z* 441.5 $[M]^+$.

4.12. 4-((E)-2-((E)-2-chloro-3-(2-((E)-7-morpholino-2-phenyl-4H-chromen-4-ylidene)ethylidene)cyclohex-1-en-1-yl)vinyl)-7-morpholino-2-phenylchromenylium perchlorate (1, FlavMorpho)

Flavylium **18** (100 mg, 0.246 mmol, 1 eq), N-[(3-(anilinomethylene)-2-chloro-1-cyclohexen-1-yl)methylene]aniline hydrochloride **23** (40 mg, 0.111 mmol, 0.45 eq) and sodium acetate (59 mg, 0.715 mmol, 2.9 eq) were dissolved in dry *n*-butanol (1.4 mL) and toluene (0.6 mL) in a flame dried flask under nitrogen atmosphere. The solution was freeze–pump–thaw 3 times and heated at 100 °C for 1 h. The crude mixture was evaporated and purified by silica gel chromatography in a gradient elution from DCM to DCM/EtOH 95:5, to give **FlavMorpho 1** (33 mg, 35 % yield) as a dark-violet solid. ^{1}H NMR (600 MHz, DMSO-d_6) δ 8.15 (d, $J = 12.7$ Hz, 2H), 8.10 (d, $J = 9.0$ Hz, 2H), 8.07 (d, $J = 6.9$ Hz,

4H), 7.59–7.54 (m, 8H), 7.14 (d, $J = 9.0$ Hz, 2H), 7.01 (d, $J = 12.1$ Hz, 4H), 3.76–3.75 (m, 8H), 3.45–3.45 (m, 8H), 2.78 (br, 4H), 1.87 (br, 2H). HRMS (ESI^+): calculated for $C_{48}H_{44}ClN_2O_4^+$ $[M]^+$: 747.2984120; found: 747.2961.

4.13. 4-((E)-2-((E)-2-chloro-3-(2-((E)-2-phenyl-7-(piperazin-1-yl)-4H-chromen-4-ylidene)ethylidene)cyclohex-1-en-1-yl)vinyl)-2-phenyl-7-(piperazin-1-yl)chromenylium perchlorate (2)

Flavylium **21** (100 mg, 0.247 mmol, 1 eq), N-[(3-(anilinomethylene)-2-chloro-1-cyclohexen-1-yl)methylene]aniline hydrochloride **23** (27 mg, 0.074 mmol, 0.3 eq) and 2,4,6-trimethylpyridine (95 μL, 0.716 mmol, 2.9 eq) were dissolved in dry *n*-butanol (1.4 mL) and toluene (0.6 mL) in a flame dried flask under nitrogen atmosphere. The solution was freeze–pump–thaw 3 times and heated to 100 °C for 5 h. The crude mixture was then evaporated under reduced pressure and the resulting solid was washed with ACN and centrifuged (3900 rpm × 10 min) 4 times. The solid was purified by reverse-phase chromatography (C8 column, gradient elution from CH_3CN + 0.1 % TFA/ H_2O + 0.1 % TFA 30:70 to 50:50) and the pure product-containing fractions were concentrated under reduced pressure and lyophilized to afford **2** (13 mg, 20 % yield) as a dark-violet solid. ^1H NMR (400 MHz, CD_3OD) δ 8.47 (d, $J = 13.9$ Hz, 2H), 8.20 (d, $J = 10.3$ Hz, 2H), 8.15–8.13 (m, 4H), 7.74 (s, 2H), 7.62–7.61 (m, 6H), 7.30 (d, $J = 9.5$ Hz, 2H), 7.23–7.20 (m, 4H), 3.82 (m, 8H), 3.43 (m, 8H), 2.90 (br, 4H), 2.03 (br, 2H). HRMS (ESI^+): calculated for $C_{48}H_{46}ClN_4O_2^+$ $[M]^+$: 745.3303809; found: 745.3311.

4.14. 4-((E)-2-((E)-2-chloro-3-(2-((E)-7-(4-methylpiperazin-1-yl)-2-phenyl-4H-chromen-4-ylidene)ethylidene)cyclohex-1-en-1-yl)vinyl)-7-(4-methylpiperazin-1-yl)-2-phenylchromenylium perchlorate (3)

Compound **19** (50 mg, 0.12 mmol, 1 eq), N-[(3-(anilinomethylene)-2-chloro-1-cyclohexen-1-yl)methylene]aniline hydrochloride **23** (17 mg, 0.048 mmol, 0.4 eq) and sodium acetate (15 mg, 0.18 mmol, 1.5 eq) were mixed in acetic anhydride (1 mL) and stirred at 80 °C in a flame dried flask under nitrogen for 2 h. The mixture was cooled to RT and DCM (3 mL) was added to the mixture to facilitate a black precipitate. The precipitate was filtered and dried under vacuum. The crude product was resuspended in hot CH_3CN/H_2O and then cooled to 0 °C for 2 h to obtain a precipitate. The obtained solid was centrifuged (3900 rpm × 10 min), washed with CH_3CN and re-centrifuged to afford **3** (9.4 mg, 22 % yield) as a dark-violet solid. ^1H NMR (400 MHz, DMSO-d_6) δ 8.31–8.28 (m, 4H), 8.25–8.19 (m, 4H), 7.83 (s, 2H), 7.64–7.64 (m, 8H), 7.29–7.26 (m, 4H), 3.16 (s, 6H), 2.88–2.86 (m, 8H), 2.75–2.71 (m, 8H), 2.66 (br, 2H), 1.89 (br, 4H). HRMS (ESI^+): calculated for $C_{50}H_{50}ClN_4O_2^+$ $[M]^+$: 773.3616810; found: 773.3478.

4.15. 7-(4-carboxypiperidin-1-yl)-4-((E)-2-((E)-3-(2-((E)-7-(4-carboxypiperidin-1-yl)-2-phenyl-4H-chromen-4-ylidene)ethylidene)-2-chlorocyclohex-1-en-1-yl)vinyl)-2-phenylchromenylium perchlorate (4)

Flavylium **20** (50 mg, 0.112 mmol, 1 eq), N-[(3-(anilinomethylene)-2-chloro-1-cyclohexen-1-yl)methylene]aniline hydrochloride **23** (18 mg, 0.05 mmol, 0.45 eq) and 2,4,6-trimethylpyridine (59 μL, 0.45 mmol, 4 eq) were dissolved in dry *n*-butanol (0.7 mL) and toluene (0.3 mL) in a flame dried flask under nitrogen atmosphere. The solution was freeze–pump–thaw 3 times and heated to 100 °C for 3 h. The crude mixture was then evaporated under reduced pressure, the resulting solid was washed with $HClO_4$ 70 % and filtered. The collected solid was purified by reverse phase chromatography (C8 column, eluent: CH_3CN + 0.1 % TFA/ H_2O + 0.1 % TFA in a gradient mode from 50:50 to 98:2) and product-containing fractions were reunited, concentrated under reduced pressure and further purified by semi-preparative reverse phase HPLC (C18 column, eluent: CH_3COONH_4 0.1 % (solvent A)/ CH_3CN (solvent B) in a gradient mode from 40 % of B to 95 % of B in 35 min; 3 mL/min; t: 65 °C; injection volume: 200 μL; product Rt: 23.6 min), followed by assaying fractions with LC-MS. Collected fractions containing the product were combined, concentrated and lyophilized twice to give **4** (9.7 mg, 21 % yield) as a dark-violet solid. HRMS (ESI^+): calculated for $C_{52}H_{48}ClN_2O_6^+$ $[M]^+$: 831.3195414; found: 831.3302. ^1H NMR characterization not available due to the very low solubility of compound **4** in common deuterated solvents.

4.16. 4-((E)-2-((E)-2-chloro-3-(2-((E)-2-phenyl-7-(4-(4-sulfobutyl) piperazin-1-yl)-4H-chromen-4-ylidene)ethylidene)cyclohex-1-en-1-yl) vinyl)-2-phenyl-7-(4-(4-sulfobutyl)piperazin-1-yl)chromenylium perchlorate (5)

Flavylium **22** (50 mg, 0.092 mmol, 1 eq), N-[(3-(anilinomethylene)-2-chloro-1-cyclohexen-1-yl)methylene]aniline hydrochloride **23** (15 mg, 0.042 mmol, 0.45 eq) and 2,6-di-*tert*-butyl-4-methylpyridine (76 mg, 0.37 mmol, 4 eq) were dissolved in dry *n*-butanol (0.7 mL) and toluene (0.3 mL) in a flame dried flask under nitrogen atmosphere. The solution was freeze–pump–thaw 3 times and heated to 100 °C for 3 h. The mixture was then evaporated under reduced pressure and purified by reverse phase chromatography (C18 column, eluent: CH_3CN + 0.1 % TFA/ H_2O + 0.1 % TFA in gradient mode starting from 70:30 to 80:20). Product-containing fractions were reunited, concentrated under reduced pressure and further purified by semi-preparative reverse phase HPLC (C18 column, eluent: CH_3COONH_4 0.1 % / CH_3CN 39:61 in isocratic mode; 3 mL/min; t: 65 °C; injection volume: 100 μL; product Rt: 5.6 min), followed by assaying fractions with LC-MS. Collected fractions containing the product were combined, concentrated and lyophilized twice to give **5** (2.4 mg, 5 % final yield) as a dark-violet solid, with a purity of 70 % at $\lambda = 254$ nm by HPLC analysis. LC-MS found [*m/z*]: 1017.3.

4.17. 1-(4-(dimethylamino)-2-hydroxyphenyl)ethan-1-one (26)

In a high-pressure reactor, 1-(4-fluoro-2-hydroxyphenyl)ethan-1-one (**7**, 1 g, 6.49 mmol, 1 eq) and dimethylamine 2.0 M in THF (**24**, 32.4 mL, 64.9 mmol, 10 eq) were mixed and stirred at 80 °C for 5 h. The solvent was then evaporated under reduced pressure and the residue was resuspended in water (20 mL) and extracted with DCM (3 × 20 mL). The combined organic phases were dried over Na_2SO_4 and concentrated under reduced pressure. The crude product was purified by silica gel chromatography (PE/AcOEt 95:5) to afford product **26** (970 mg, 83 % yield) as a white solid. ^1H NMR (600 MHz, $CDCl_3$) δ 12.88 (s, 1H), 7.53 (d, $J = 9.0$ Hz, 1H), 6.20 (dd, $J = 9.1$, 2.6 Hz, 1H), 6.08 (d, $J = 2.8$ Hz, 1H), 3.04 (s, 6H), 2.49 (s, 3H). ^{13}C NMR (151 MHz, $CDCl_3$) δ 200.8, 164.8, 155.8, 132.3, 110.2, 103.8, 97.7, 39.9, 25.6. MS (ESI^+): *m/z* 180.3 $[M + H]^+$.

4.18. 2-((4-acetyl-3-hydroxyphenyl)(methyl)amino)ethane-1-sulfonic acid (27)

In a screw-capped vial, to a solution of *N*-methyl taurine **25** (181 mg, 1.30 mmol, 4 eq) in DMF (2 mL), 1-(4-fluoro-2-hydroxyphenyl)ethan-1-one **7** (50 mg, 0.324 mmol, 1 eq) and K_2CO_3 (45 mg, 0.324 mmol, 1 eq) were added and the reaction was stirred at 110 °C for 24 h. The mixture was cooled to RT and filtered, the solid was washed with DCM (5 mL) and the filtrate was concentrated under reduced pressure. The crude product was purified by silica gel chromatography (DCM/MeOH 8:2) to afford **27** (71 mg, 80 % yield) as a whitish solid. ^1H NMR (600 MHz, CD_3OD) δ 7.65 (dd, $J = 9.1$, 1.2 Hz, 1H), 6.37–6.35 (m, 1H), 6.10 (d, $J = 2.4$ Hz, 1H), 3.84 (t, $J = 7.7$ Hz, 2H), 3.08–3.05 (m, 5H), 2.47 (s, 3H). ^{13}C NMR (151 MHz, CD_3OD) δ 202.8, 166.1, 156.3, 134.1, 111.4, 105.3, 98.5, 49.1, 48.7, 38.7, 25.6. MS (ESI^-): *m/z* 272.2 $[M]^-$.

4.19. 7-(dimethylamino)-4-methyl-2-phenylchromenylium perchlorate (28)

Compound **26** (400 mg, 2.23 mmol, 1 eq) and acetophenone **17** (1.2 mL, 10.3 mmol, 4.6 eq) were dissolved in acetic acid (8.6 mL) and perchloric acid 70 % (4.3 mL) was added dropwise at room temperature. The reaction was stirred at 105 °C for 20 h under a nitrogen atmosphere. After being cooled to room temperature, water was added to the mixture to facilitate a violet precipitate. The precipitate was filtered, washed with diethyl ether, and dried under vacuum to obtain compound **28** (612 mg, 75 % yield) which was used in the following step without further purification. ^{1}H NMR (600 MHz, CD_3OD) δ 8.32 (d, $J = 7.6$ Hz, 2H), 8.19 (d, $J = 9.6$ Hz, 1H), 7.99 (s, 1H), 7.74–7.72 (m, 1H), 7.67 (t, $J = 7.7$ Hz, 2H), 7.50 (dd, $J = 9.6$, 2.4 Hz, 1H), 7.25 (d, $J = 2.4$ Hz, 1H), 3.39 (s, 6H), 2.91 (s, 3H). MS (ESI$^+$): *m/z* 264.4 $[M]^+$.

4.20. 4-methyl-7-(methyl(2-sulfoethyl)amino)-2-phenylchromenylium perchlorate (29)

Compound **27** (60 mg, 0.22 mmol, 1 eq) and acetophenone **17** (102 μL, 0.88 mmol, 4 eq) were dissolved in acetic acid (1 mL), and perchloric acid 70 % (0.5 mL) was added dropwise at room temperature. The reaction was stirred at 105 °C for 20 h under a nitrogen atmosphere. After being cooled to room temperature, water was added (10 mL) and the aqueous phase was extracted with DCM/MeOH (2 × 10 mL) and *n*-BuOH (2 × 10 mL). The combined organic phases were concentrated under reduced pressure until the formation of a red precipitate, which was filtered and dried under vacuum to afford **29** (30 mg, 30 % yield) as an orange-red solid. The product was used in the following step without further purification. ^{1}H NMR (600 MHz, CD_3OD) δ 8.32 (d, $J = 7.4$ Hz, 2H), 8.19 (d, $J = 9.6$ Hz, 1H), 8.01 (s, 1H), 7.73 (t, $J = 7.2$ Hz, 1H), 7.66 (t, $J = 7.4$ Hz, 2H), 7.54 (s, 1H), 7.30 (s, 1H), 4.12 (t, $J = 6.9$ Hz, 2H), 3.39 (s, 3H), 3.20 (t, $J = 6.9$ Hz, 2H), 2.91 (s, 3H). MS (ESI$^+$): *m/z* 358.4 $[M]^+$.

4.21. 4-((E)-2-((E)-2-chloro-3-(2-((E)-7-(dimethylamino)-2-phenyl-4H-chromen-4-ylidene)ethylidene)cyclohex-1-en-1-yl)vinyl)-7-(dimethylamino)-2-phenylchromenylium perchlorate (Flav7)

Flavylium **28** (50 mg, 0.137 mmol, 1 eq), N-[(3-(anilinomethylene)-2-chloro-1-cyclohexen-1-yl)methylene]aniline hydrochloride **23** (22 mg, 0.062 mmol, 0.45 eq) and sodium acetate (33 mg, 0.399 mmol, 2.9 eq) were dissolved in dry *n*-butanol (0.7 mL) and toluene (0.3 mL) in a flame dried flask under nitrogen atmosphere. The solution was freeze–pump–thaw 3 times and heated to 100 °C for 30 min. The crude mixture was evaporated and purified by silica gel chromatography (gradient mode from DCM to DCM/EtOH 97:3). After a second chromatographic purification on silica gel (gradient mode from DCM/EtOAc 7:3 switching to DCM/EtOH 9:1) **Flav7** was obtained as a violet solid (14 mg, 30 % yield). ^{1}H NMR (600 MHz, DMSO-d_6) δ 8.16 (d, $J = 14.2$ Hz, 2H), 8.08 (d, $J = 6.9$ Hz, 6H), 7.59–7.55 (m, 8H), 7.01 (d, $J = 13.3$ Hz, 2H), 6.93 (d, $J = 6.9$ Hz, 2H), 6.76 (d, $J = 4.8$ Hz, 2H), 3.12 (s, 12H), 2.80 (br, 4H), 1.90–1.87 (m, 2H). HRMS (ESI +): calculated for $C_{44}H_{40}ClN_2O_2^+$ $[M]^+$: 663.2772827; found: 663.2709.

4.22. 4-((E)-2-((E)-2-chloro-3-(2-((E)-7-(methyl(2-sulfoethyl)amino)-2-phenyl-4H-chromen-4-ylidene)ethylidene)cyclohex-1-en-1-yl)vinyl)-7-(methyl(2-sulfoethyl)amino)-2-phenylchromenylium perchlorate (6)

Flavylium **29** (27 mg, 0.059 mmol, 1 eq), N-[(3-(anilinomethylene)-2-chloro-1-cyclohexen-1-yl)methylene]aniline hydrochloride **23** (9.5 mg, 0.027 mmol, 0.45 eq) and 2,6-di-*tert*-butyl-4-methylpyridine (48 mg, 0.24 mmol, 4 eq) were dissolved in dry *n*-butanol (0.7 mL) and toluene (0.3 mL) in a flame dried flask under nitrogen atmosphere. The solution was freeze–pump–thaw 3 times and heated to 100 °C for 4 h. The crude mixture was then evaporated under reduced pressure and the crude product was purified by semi-preparative reverse phase HPLC (C18 column, eluent: CH_3COONH_4 0.1 % / EtOH 96 % 40:60 in isocratic mode; 3 mL/min; t: 65 °C; injection volume: 100 μL; product Rt: 10.4 min), followed by assaying fractions with LC-MS. Collected fractions containing the product were combined, concentrated and lyophilized twice to give **6** (1.7 mg, 7 % yield) as a dark-violet solid, with a purity of 82 % at $\lambda = 254$ nm by HPLC analysis. LC-MS found [*m/z*]: 851.2.

4.23. Photophysical characterization

Absorption spectra in different solvents were obtained of diluted dye solutions in a 1 cm cuvette. From the baseline corrected and normalized data, the maximum absorption wavelength ($\lambda_{max,\ abs}$) values were obtained. Displayed normalized spectra are normalized to 1.0. Emission spectra were obtained of diluted dye solutions in different solvents in a 1 cm cuvette, with excitation wavelength of $\lambda = 870$ nm. From the baseline corrected and normalized data, the maximum emission wavelength ($\lambda_{max,\ em}$) values were obtained. Displayed spectra are normalized to 1.0. Emission tails in SWIR region were recorded from 1040 to 1400 nm by using $\lambda = 808$ nm or $\lambda_{max,\ abs}$ as excitation wavelength. Integrals values of the emission tails were calculated by Origin. All spectra were obtained at ambient temperature.

Absorption coefficients in DCM were determined by linear regression of the absorbance vs the concentration of the dye solution, obtained with serial dilutions in volumetric glassware. Absolute fluorescence quantum yield measurements were taken on the FluoroLog-3 1IHR-320 spectrofluorometer with 450 W Xenon Light source and equipped with an F-3018 integrating sphere accessory (Horiba Jobin Yvon). Detection was performed by photomultiplier tubes (PMT-NIR, R5509) cooled detector. Measurements are reported as the average ± standard deviation of 3 replicate measurements. For quantum yield measurements, samples were excited with 870 nm wavelength and collected between 1000–1250 nm. Slit widths were 1.3 nm excitation/emission with 1 nm step size and 0.1 s integration time. The excitation light was collected between 860–880 nm. Optical densities of all samples were below 0.1 to minimize effects of reabsorption.

4.24. Stability studies and spectral monitoring of monomer – aggregate equilibrium

Absorption spectra of each compound in ACN and ACN + 10 % water were repeatedly recorded over a period of 200 min. Spectra were scanned at a controlled temperature of 25 °C and at 6-minute intervals. The first spectrum was recorded immediately after the solution was prepared and represented "t = 0 min" spectrum. Absorbance was monitored at the maximum absorption wavelength of t = 0 min in correspondence of both the monomer and the aggregate peak, and the residual absorbance (%) at fixed time points was calculated with respect to the absorbance values at t = 0 min (100 %).

4.25. Encapsulation of dyes in phospholipidic micelles

The lipid, mPEG-DSPE (11 mg) (PEG 18:0 PE 2000), was dissolved in MilliQ water (2.0 mL), sonicated with a probe sonicator until complete dissolution and kept on an ice bath at 0 °C. **Flav7** or **FlavMorpho** (**1**) (0.11 mg for 1 % wt micelles; 0.22 mg for 2 % wt micelles; 0.44 mg for 4 % wt micelles) were dissolved in DMSO (1.0 mL), and these solutions were added to the aqueous solution of the lipid at 0 °C. The resulting mixture was sonicated with a probe sonicator at 35 % power for 5 min at 0 °C. The solution was then transferred to a 4 mL centrifuge filter (10 kDa, Amicon) and 6 sequential centrifugations (4000 rpm × 10 min) were performed, replacing the filtered solvent with 1x PBS buffer. The micelles were then concentrated by centrifugation (4000 rpm × 5 min) to a final volume of around 1.0 mL, filtered through 0.22 μm syringe filters (Millex-GS 0.22 μm, Merck) and diluted with 1x PBS to a final volume of 2.0 mL. For the vehicle, the exact same procedure was

followed but without the addition of dye. Micelle solutions in PBS were stored at 4 °C. The size of the micelle formulations was determined by dynamic light scattering (DLS) analysis at 25 °C, using an equilibration time of 300 s. Data are representative of 3 replicate measurements.

4.26. Determination of dye concentration within micelles

The concentration of dyes within the micelles was determined spectrophotometrically and interpolated from a standard curve. First, serial dilutions of **Flav7** or **FlavMorpho (1)** in a mixture of DCM/MeOH 1:1 in the presence of mPEG-DSPE (2.75 mg in 0.5 mL of solution) were analyzed to derive a standard curve. The absorption coefficients were determined under these conditions and used to obtain the concentration of the dyes within the micelles (diluted in DCM/MeOH 1:1 and analyzed with the spectrophotometer) by applying the Beer-Lambert law. Once defined the actual concentration of encapsulated dye, the micelles were diluted to a final concentration of 20 μM and UV/Vis/NIR spectroscopy and fluorescence spectroscopy were performed as described in the general experimental procedures (see 4.23 section). Measurements were performed in PBS and a clinical chemistry quality control human serum (Seronorm, Sero SA).

4.27. Brightness comparison using SWIR imaging device

To verify and compare the performance of dyes, minimum detectable concentrations were evaluated with the SWIR imaging system by varying micelle-loaded fluorophore concentration (0.1 to 20 μM) in PBS and human serum (Seronorm, Sero SA). Diluted solutions were transferred to Eppendorf tubes and imaged with the SWIR apparatus equipped with an excitation light LED arrays at 808 nm, selecting GAIN 1 and 150 ms of exposure time. The images of Eppendorf tubes were acquired using a cooled InGaAs camera (Goldeye G-032 SWIR Cool TEC2 FPA; 640 × 8512 pixel, 4/3″Allied Vision Technologies, Germany), the emitted light was passed through Thorlabs FELH 1100 long-pass filter, and a sample of PBS or serum alone was used as a control. Captured images were processed with ImageJ for the definition of the region of interest (ROI) to calculate the signal-to-noise ratio (SNR). The limit of detection (LOD) was calculated as three times the SNR, while the limit of quantification (LOQ) was calculated as ten times the SNR.

CRediT authorship contribution statement

Federica Blua: Writing – original draft, Visualization, Investigation. **Mariangela Boccalon:** Methodology, Investigation. **Barbara Rolando:** Methodology. **Roberta Napolitano:** Writing – review & editing, Supervision, Resources, Funding acquisition, Conceptualization. **Francesca Arena:** Investigation. **Francesco Blasi:** Writing – review & editing, Supervision, Project administration, Conceptualization. **Massimo Bertinaria:** Writing – review & editing, Supervision, Project administration, Funding acquisition, Conceptualization.

Declaration of competing interest

The authors declare that they have no known competing financial interests or personal relationships that could have appeared to influence the work reported in this paper.

Acknowledgments

This work was supported by University of Turin, Ricerca Locale 2021, (BERM_RILO_21_01). We thank Consiglio Nazionale delle Ricerche (CNR) and Bracco Imaging S.p.A for funding a PhD grant to FB.

Appendix A. Supplementary data

Supplementary data to this article can be found online at https://doi.org/10.1016/j.bioorg.2024.107462.

References

[1] G. Pirovano, S. Roberts, S. Kossatz, T. Reiner, Optical imaging modalities: Principles and applications in preclinical research and clinical settings, J. Nucl. Med. 61 (2020) 1419–1427, https://doi.org/10.2967/jnumed.119.238279.
[2] A. Refaat, M.L. Yap, G. Pietersz, A.P.G. Walsh, J. Zeller, B. del Rosal, X. Wang, K. Peter, In vivo fluorescence imaging: success in preclinical imaging paves the way for clinical applications, J. Nanobiotechnol. 20 (2022), https://doi.org/10.1186/s12951-022-01648-7.
[3] H.M. Schouw, L.A. Huisman, Y.F. Janssen, R.H.J.A. Slart, R.J.H. Borra, A.T. M. Willemsen, A.H. Brouwers, J.M. van Dijl, R.A. Dierckx, G.M. van Dam, W. Szymanski, H.H. Boersma, S. Kruijff, Targeted optical fluorescence imaging: a meta-narrative review and future perspectives, Eur. J. Nucl. Med. Mol. Imaging 48 (2021) 4272–4292, https://doi.org/10.1007/s00259-021-05504-y.
[4] K. Wang, Y. Du, Z. Zhang, K. He, Z. Cheng, L. Yin, D. Dong, C. Li, W. Li, Z. Hu, C. Zhang, H. Hui, C. Chi, J. Tian, Fluorescence image-guided tumour surgery, Nat. Rev. Bioeng. 1 (2023) 161–179, https://doi.org/10.1038/s44222-022-00017-1.
[5] S. Van Keulen, M. Hom, H. White, E.L. Rosenthal, F.M. Baik, The evolution of fluorescence-guided surgery, Mol. Imag. Biol. 25 (2023) 36–45, https://doi.org/10.1007/s11307-022-01772-8.
[6] J.S.D. Mieog, F.B. Achterberg, A. Zlitni, M. Hutteman, J. Burggraaf, R. J. Swijnenburg, S. Gioux, A.L. Vahrmeijer, Fundamentals and developments in fluorescence-guided cancer surgery, Nat. Rev. Clin. Oncol. 19 (2022) 9–22, https://doi.org/10.1038/s41571-021-00548-3.
[7] G. Hong, A.L. Antaris, H. Dai, Near-infrared fluorophores for biomedical imaging, Nat. Biomed. Eng. 1 (2017) 0010, https://doi.org/10.1038/s41551-016-0010.
[8] Y. Chen, S. Wang, F. Zhang, Near-infrared luminescence high-contrast in vivo biomedical imaging, Nat. Rev. Bioeng. 1 (2023) 60–78, https://doi.org/10.1038/s44222-022-00002-8.
[9] K. Welsher, Z. Liu, S.P. Sherlock, J.T. Robinson, Z. Chen, D. Daranciang, H. Dai, A route to brightly fluorescent carbon nanotubes for near-infrared imaging in mice, Nat. Nanotechnol. 4 (2009) 773–780, https://doi.org/10.1038/nnano.2009.294.
[10] H. Dai, Q. Shen, J. Shao, W. Wang, F. Gao, X. Dong, Small Molecular NIR-II Fluorophores for Cancer Phototheranostics, The Innovation 2 (2021) 100082, https://doi.org/10.1016/j.xinn.2021.100082.
[11] F. Ding, Y. Fan, Y. Sun, F. Zhang, Beyond 1000 nm emission wavelength: recent advances in organic and inorganic emitters for deep-tissue molecular imaging, Adv. Healthc. Mater. 8 (2019), https://doi.org/10.1002/adhm.201900260.
[12] S. Zhu, R. Tian, A.L. Antaris, X. Chen, H. Dai, Near-infrared-II molecular dyes for cancer imaging and surgery, Adv. Mater. 31 (2019) 1900321, https://doi.org/10.1002/adma.201900321.
[13] S. Wang, B. Li, F. Zhang, Molecular fluorophores for deep-tissue bioimaging, ACS Cent. Sci. 6 (2020) 1302–1316, https://doi.org/10.1021/acscentsci.0c00544.
[14] Y.-F. Ou, T.-B. Ren, L. Yuan, X.-B. Zhang, Molecular design of NIR-II polymethine fluorophores for bioimaging and biosensing, Chem. Biomed. Imaging 1 (2023) 220–233, https://doi.org/10.1021/cbmi.3c00040.
[15] X. Feng, L. Wei, Y. Liu, X. Chen, R. Tian, Orchestrated strategies for developing fluorophores for NIR-II imaging, Adv. Healthc. Mater. 12 (2023) 2300537, https://doi.org/10.1002/adhm.202300537.
[16] Z. Lei, F. Zhang, Molecular engineering of NIR-II fluorophores for improved biomedical detection, Angew. Chem. Int. Ed. 60 (2021) 16294–16308, https://doi.org/10.1002/anie.202007040.
[17] J. Mu, M. Xiao, Y. Shi, X. Geng, H. Li, Y. Yin, X. Chen, The chemistry of organic contrast agents in the NIR-II window, Angew. Chem. Int. Ed. 61 (2022) e202114722.
[18] X. Zhao, F. Zhang, Z. Lei, The pursuit of polymethine fluorophores with NIR-II emission and high brightness for in vivo applications, Chem. Sci. 13 (2022) 11280–11293, https://doi.org/10.1039/d2sc03136a.
[19] Y. Du, X. Liu, S. Zhu, Near-infrared-II cyanine/polymethine dyes, current state and perspective, Front. Chem. 9 (2021), https://doi.org/10.3389/fchem.2021.718709.
[20] S. Zhu, R. Tian, A.L. Antaris, X. Chen, H. Dai, Near-infrared-II molecular dyes for cancer imaging and surgery, Adv. Mater. 31 (2019), https://doi.org/10.1002/adma.201900321.
[21] E.D. Cosco, J.R. Caram, O.T. Bruns, D. Franke, R.A. Day, E.P. Farr, M.G. Bawendi, E.M. Sletten, Flavylium polymethine fluorophores for near- and shortwave infrared imaging, Angew. Chem. 129 (2017) 13306–13309, https://doi.org/10.1002/ange.201706974.
[22] S. Wang, Y. Fan, D. Li, C. Sun, Z. Lei, L. Lu, T. Wang, F. Zhang, Anti-quenching NIR-II molecular fluorophores for in vivo high-contrast imaging and pH sensing, Nat. Commun. 10 (2019), https://doi.org/10.1038/s41467-019-09043-x.
[23] Z. Lei, C. Sun, P. Pei, S. Wang, D. Li, X. Zhang, F. Zhang, Stable, wavelength-tunable fluorescent dyes in the NIR-II region for in vivo high-contrast bioimaging and multiplexed biosensing, Angew. Chem. 131 (2019) 8250–8255, https://doi.org/10.1002/ange.201904182.
[24] E.D. Cosco, A.L. Spearman, S. Ramakrishnan, J.G.P. Lingg, M. Saccomano, M. Pengshung, B.A. Arús, K.C.Y. Wong, S. Glasl, V. Ntziachristos, M. Warmer, R. R. McLaughlin, O.T. Bruns, E.M. Sletten, Shortwave infrared polymethine fluorophores matched to excitation lasers enable non-invasive, multicolour in vivo imaging in real time, Nat. Chem. 12 (2020) 1123–1130, https://doi.org/10.1038/s41557-020-00554-5.
[25] E.D. Cosco, B.A. Arús, A.L. Spearman, T.L. Atallah, I. Lim, O.S. Leland, J.R. Caram, T.S. Bischof, O.T. Bruns, E.M. Sletten, Bright chromenylium polymethine dyes

enable fast, four-color in vivo imaging with shortwave infrared detection, J. Am. Chem. Soc. 143 (2021) 6836–6846, https://doi.org/10.1021/jacs.0c11599.
[26] S. Ma, S. Du, G. Pan, S. Dai, B. Xu, W. Tian, Organic molecular aggregates: From aggregation structure to emission property, Aggregate 2 (2021) e96.
[27] D. Zhai, W. Xu, L. Zhang, Y.T. Chang, The role of "disaggregation" in optical probe development, Chem. Soc. Rev. 43 (2014) 2402–2411, https://doi.org/10.1039/c3cs60368g.
[28] J. Qi, X. Hu, X. Dong, Y. Lu, H. Lu, W. Zhao, W. Wu, Towards more accurate bioimaging of drug nanocarriers: turning aggregation-caused quenching into a useful tool, Adv. Drug Deliv. Rev. 143 (2019) 206–225, https://doi.org/10.1016/j.addr.2019.05.009.
[29] M. Pengshung, J. Li, F. Mukadum, S.A. Lopez, E.M. Sletten, Photophysical tuning of shortwave infrared flavylium heptamethine dyes via substituent placement, Org. Lett. 22 (2020) 6150–6154, https://doi.org/10.1021/acs.orglett.0c02213.
[30] Y. Qiu, H. Hu, D. Zhao, J. Wang, H. Wang, Q. Wang, H. Peng, Y. Liao, X. Xie, Concentration-dependent dye aggregation and disassembly triggered by the same artificial helical foldamer, Polymer (Guildf) 170 (2019) 7–15, https://doi.org/10.1016/j.polymer.2019.02.063.
[31] J.A. Carr, D. Franke, J.R. Caram, C.F. Perkinson, M. Saif, V. Askoxylakis, M. Datta, D. Fukumura, R.K. Jain, M.G. Bawendi, O.T. Bruns, Shortwave infrared fluorescence imaging with the clinically approved near-infrared dye indocyanine green, PNAS 115 (2018) 4465–4470, https://doi.org/10.1073/pnas.1718917115.
[32] S. Zhu, B.C. Yung, S. Chandra, G. Niu, A.L. Antaris, X. Chen, Near-Infrared-II (NIR-II) bioimaging via Off-Peak NIR-I fluorescence emission, Theranostics 8 (2018) 4141–4151, https://doi.org/10.7150/thno.27995.
[33] E.D. Cosco, I. Lim, E.M. Sletten, Photophysical properties of indocyanine green in the shortwave infrared region, ChemPhotoChem 5 (2021) 727–734, https://doi.org/10.1002/cptc.202100045.
[34] F. Arena, F. La Cava, D. Faletto, M. Roberto, F. Crivellin, F. Stummo, A. Adamo, M. Boccalon, R. Napolitano, F. Blasi, M. Koch, A. Taruttis, E. Reitano, Short-wave infrared fluorescence imaging of near-infrared dyes with robust end-tail emission using a small-animal imaging device, PNAS Nexus 2 (2023), https://doi.org/10.1093/pnasnexus/pgad250.
[35] X. Wu, Y. Suo, H. Shi, R. Liu, F. Wu, T. Wang, L. Ma, H. Liu, Z. Cheng, Deep-tissue photothermal therapy using laser illumination at NIR-IIa window, Nanomicro. Lett. 12 (2020), https://doi.org/10.1007/s40820-020-0378-6.
[36] W. Wang, X. He, M. Du, C. Xie, W. Zhou, W. Huang, Q. Fan, Organic fluorophores for 1064 nm excited NIR-II fluorescence imaging, Front. Chem. 9 (2021) 769655, https://doi.org/10.3389/fchem.2021.769655.
[37] S. Jia, E.Y. Lin, E.B. Mobley, I. Lim, L. Guo, S. Kallepu, P.S. Low, E.M. Sletten, Water-soluble chromenylium dyes for shortwave infrared imaging in mice, Chem 9 (2023) 3648–3665, https://doi.org/10.1016/j.chempr.2023.08.021.